Universität Stuttgart
Geodätisches Institut

Comparison between gravity gradients from dense CryoSat-2 altimetry and from shipborne gradiometry

Bachelorarbeit im Studiengang
Geodäsie & Geoinformatik
an der Universität Stuttgart

Roman Buss

Stuttgart, Dezember 2017

Betreuer: Prof. Dr.-Ing. Nico Sneeuw
Universität Stuttgart

Erklärung der Urheberschaft

Ich erkläre hiermit an Eides statt, dass ich die vorliegende Arbeit ohne Hilfe Dritter und ohne Benutzung anderer als der angegebenen Hilfsmittel angefertigt habe; die aus fremden Quellen direkt oder indirekt übernommenen Gedanken sind als solche kenntlich gemacht. Die Arbeit wurde bisher in gleicher oder ähnlicher Form in keiner anderen Prüfungsbehörde vorgelegt und auch noch nicht veröffentlicht.

Ort, Datum Unterschrift

Abstract

Satellite altimetry is a tool to gather information about Earth's oceans and ice coverage on a global extent. Altimetric data can be used to monitor ice sheet changes, create bathymetric maps or analyze the sea surface. Extensive comprehension of the vast masses of water on Earth will benefit not only geodetic but also various scientific aspects.

This paper will deal with altimetric data collected by ESA's satellite CryoSat-2. The satellite is designed to perform measurements of both ocean surface and ice sheets. Vertical gravity gradients will be calculated on the basis of sea surface height measurement.

The area of interest is located between Faroe Islands and Shetland Islands north of Scotland. The created vertical gravity gradients will be compared with a dataset collected by Bell Geospace via shipborne gradiometry. Satellite altimetry enables a rather convenient acquisition of global data compared to traditional gradiometric methods.

The main objective is to find out whether satellite altimetry is a viable alternative to generate gravity gradient data on a global extent.

Contents

1 Introduction **1**
1.1 Thesis Objectives . . . 1
1.2 About CryoSat Mission . . . 1
1.2.1 Orbit . . . 2
1.2.2 Operation Modes and Footprint . . . 4

2 Data **7**
2.1 CryoSat-2 Data Availability . . . 7
2.2 Recondition of the data . . . 8
2.3 FTG Data . . . 10
2.3.1 Overview . . . 10
2.3.2 Description and Accuracy . . . 11

3 Computations **15**
3.1 Vertical Gravity Gradients From Deflections Of The Vertical . . . 15
3.2 Interpolation . . . 20
3.2.1 Point Distribution . . . 20
3.2.2 Inverse Distance Weighting Interpolation . . . 22
3.3 Comparison . . . 25
3.3.1 Exemplaric Analysis . . . 28

4 Conclusion **31**

A Appendix **XV**

List of Figures

1.1 CryoSat-2 Ground-Track Sample . . . 3
1.2 Pulse-Limited-footprint for LRM, Source: (Footprint 2013) . . . 5
1.3 Pulse-Doppler-limited footprint for SAR/SARin, Source: (Footprint 2013) . . . 6

2.1 Mode Mask, Source: (CryoSat Mode Mask) . . . 7
2.2 Basic altimetry terms and functions, Source: (CS Product Handbook 2014) . . . 8
2.3 Sample of satellite tracks within area of interest . . . 9
2.4 Area surveyed by shipborne gradiometry, Source: (Roth 2009) . . . 10
2.5 Sample of trajectories of FTG measurements . . . 11
2.6 Closeup of FTG . . . 12
2.7 Vertical Gravity Gradient T_{zz} from FTG . . . 13

3.1 Distribution of altimetric crossover points and FTG-points . . . 20
3.2 Favourable Crossover Point Distribution . . . 21
3.3 Unfavourable Crossover Point Distribution . . . 21
3.4 Search window: Small with box edge 0.01 ° , large with box edge 0.05 ° . . . 23
3.5 Closeup of Search Window area with box edge 0.01 ° . . . 24
3.6 Histogram of $\frac{\partial \Delta g}{\partial z} - T_{zz}$ . . . 25
3.7 Closeup of Histogram in figure 3.6 . . . 26
3.8 Histograms for altimetric and gradiometric vertical gravity gradients . . . 27
3.9 Lines 56 and 68 in the Difference Field . . . 28
3.10 Along track course of Line 68 . . . 29
3.11 Course of Line 56 with respect to Latitude . . . 29

A.1 Latitudinal ground-track velocities . . . XV
A.2 Longitudinal ground-track velocities . . . XVI
A.3 Histogram for ratios of ascending and descending longitudinal ground track velocities . . . XVI
A.4 Histogram for ratios of ascending and descending latitudinal ground track velocities . . . XVII

Chapter 1

Introduction

1.1 Thesis Objectives

This thesis will deal with altimetric data collected by ESA's satellite CryoSat-2. Since satellite altimetry data provided by ESA is rather easy to handle and reliable, altimetriy is an encouraging source for research on a global scale. It will be attempted to compute gravity gradients on the basis of position and ocean surface height measurements. Gravity gradients indicate gravity changes in the direction of the respective coordinate axes. Moreover, the vertical gravity gradient is of particular importance in the interpretation of gravity data. The area of interest is located between Faroe Islands and Shetland Islands north of Scotland. The area was chosen because of a given record of Full Tensor Gradiometry data by Bell Geospace, which was collected via shipborne gradiometry.

After an introduction about the satellite and its characteristics in sections 1.2.1 and 1.2.2 the given datasets will be discussed in Chapter 2. The next step is to perform computations of the deflection of the vertical leading to determination of vertical gravity gradients in section 3.1. Afterwards the vertical gravity gradients will be interpolated onto the gradiometric dataset in section 3.2 to allow comparison in section 3.3.

1.2 About CryoSat Mission

The CryoSat mission is part of the 'Living Planet' programme of the European Space Agency. It consists of a satellite designed to monitor sea and land ice variations on a global scale, in order to determine mass fluctuations of Earth's major land and marine ice fields. Knowledge of these fluctuations can help predicting future sea level and climate. The mission originally was set to launch in 2005 but due to failure in the launch vehicle the satellite got destroyed. Therefore, the now operating satellite is CryoSat-2, launched in 2010, consisting of the same hardware component as CryoSat. Also the mission goal remained identical (CS Science and Mission 1999).

As the satellite crosses the open oceans it operates as a high spatial resolution radar altimeter i.e. measuring height of the ocean surface. The altimetry data is collected with CryoSat's primary instrument: the Synthetic Aperture Radar / Interferometric Radar Altimeter (SIRAL). The satellite can operate in three different modes, depending on the various surfaces beneath it. The two modes concerning the used dataset in this paper will be explained under subsection 1.2.2

1.2.1 Orbit

Crucial for CryoSat's function is the orbit it operates on. Its inclination is designed to satisfy the needs between density of orbit tracks and coverage of very high latitude regions. However, the orbit is not polar which leads to a precession of the nodal plane at a rate of approximately 0.25° per day. On the one hand, the satellite therefore is exposed to long periods of constant sunlight along the dawn-dusk line. On the other hand, CryoSat faces periods of low solar radiation along the noon-midnight plane (CS Science and Mission 1999).

Furthermore, the altitude exposes the satellite to various effects such as air-drag or sun and moon activity. If these effects will not be compensated the semi-major axis of the orbit will continuously decay, which results in a ground track error reaching some km in about 10 days. For a stable operation it is therefore necessary, that CryoSat's orbit is maintained throughout the whole mission. To ensure reliable and accurate orbit determination CryoSat uses the common Doppler Orbitography and Radiopositioning Integrated by Satellite (DORIS) technology. DORIS performs measurements of the relative velocity to a global network of ground stations using the Doppler Effect.

Figure 1.1 displays the ground track of the satellite for one day. The effect of the high latitude inclination is noticeable. Also, the course of the ground tracks in north-south direction appears to be steep, which is intended to reach a dense coverage of ascending and descending tracks. Within one day CryoSat-2 performs 14.5 revolutions on the average.

A proper knowledge of CryoSat's orbit is inevitable for general comprehension of this topic and further computations. Computation procedures rely not only on accurate, but also on a sufficient amount of position and height data. The repeat period of CryoSat-2 is rather long with 369 days, thus it will take more than a year for the satellite to pass the same spot on earth surface. On the one hand, casual changes in a certain area can not be observed regularly. On the other hand, the repeat period enables a short inter-track-spacing. With its 7.5 km the satellite creates a dense grid of ascending and descending tracks. Thus, one is enabled to obtain a great amount of data with fine gaps between the tracks.
This thesis will analyze if the density of data leads to a gravity gradient model comparable to shipborne gradiometrty.

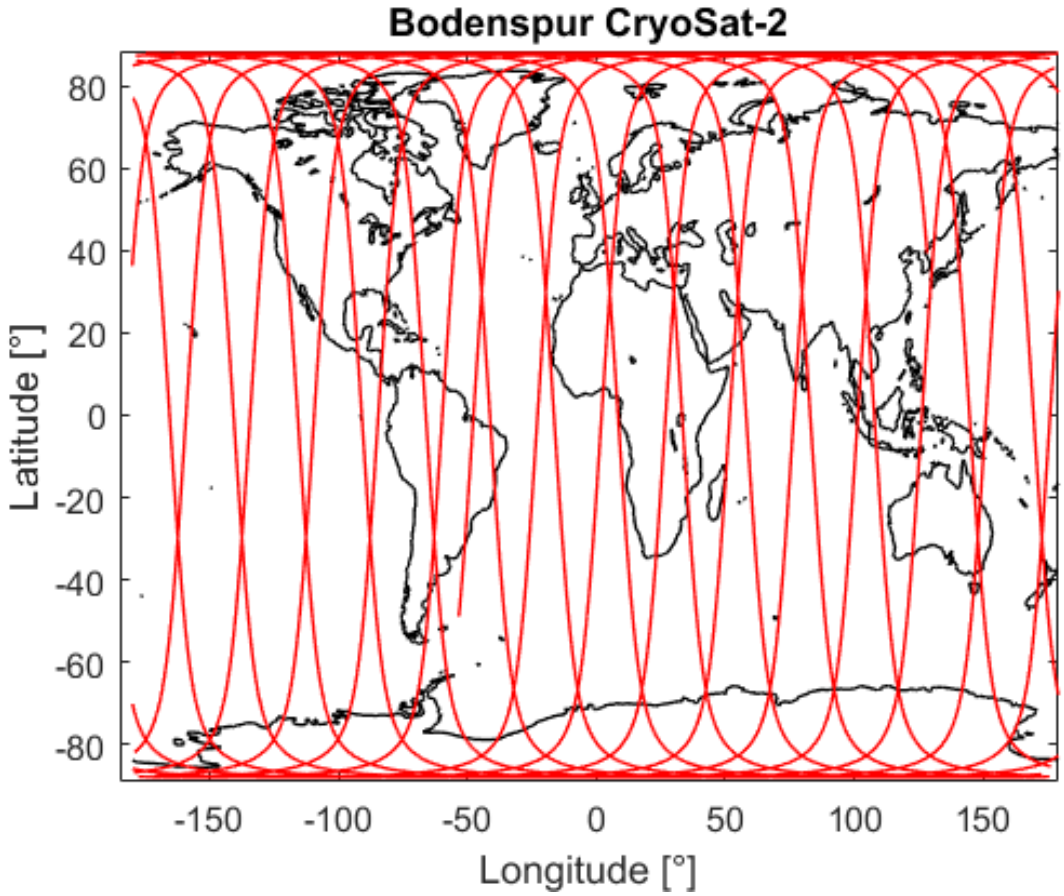

Figure 1.1: *CryoSat-2 Ground-Track Sample*

Type	near-circular, polar, low-earth orbit
Mean altitude	717.2 km
Repeat period	369 day with 30 day sub-cycle
Inter-track-spacing	7.5 km at equator
Orbit Control	±5 km
Longitude of equator crossing	*TDB*

Keplerian elements

Semi-Major axis a	7095.4 km
Eccentricity e	0.0014
Inclination i	92.001 °
Right Ascension Ω	129.997 °
Argument of Perigee ω	115.619 °
True Anomaly M	283.899 °

1.2.2 Operation Modes and Footprint

CryoSat is capable of three different operation modes depending on the surface beneath the satellite. The two modes relevant for this thesis will be analyzed in this subsection.
Over open ocean the satellites operates as a traditional radar altimeter, whereas over sea ice CryoSat uses SAR. Over land ice masses such as glaciers, the most advanced mode, SARIN is used. Each operation mode has an individual footprint. Footprint is the technical term for the area covered by the satellite's beam. The reasulting echoes are collected and processed in order to become measuring data. The size and form of the footprint is determined by the satellite's altitude and antenna pattern. Along-track and across-track direction of the footprint are a result of form, which itself is determined by the operation mode. Naturally, a higher altitude results in a smaller footprint, whereas a lower altitude leads to a larger footprint. The following paragraphs will deal with the pulse-limited footprint. This technique is used for collecting LRM and SAR data (Footprint 2013).

- Pulse-limited footprint for LRM

  The pulse-limited footprint depends on time delay. The pulse-limited footprint is defined as the illuminated area on the ground around the point of closest approach. It corresponds to the area illuminated by the leading edge of the pulse until the trailing edge first intersects the surface. Full illumination is given when the rear of the pulse reaches the sea. The greater the delaying time, the larger the radius of the illuminated area is. The footprint is defined as:

  $$r = \sqrt{h \cdot c \cdot \tau} = \sqrt{h \cdot \frac{c}{B}}$$

  where

  $$\begin{aligned} &c - \text{speed of light} = 299792458 \frac{\text{m}}{\text{s}} \\ &h - \text{average altitude} = 730\,\text{km} \\ &\tau - \text{compressed pulse length} = \frac{1}{B} \\ &B - \text{pulse bandwidth} = 320\,\text{MHz} \end{aligned}$$

  Using the given standard values for these parameters, the calculated radius is $r_{\text{pulse}} = 0.827\,\text{km}$, hence diameter is $D_{\text{pulse}} = 1.65\,\text{km}$. Therefore, the covered area of the footprint is 2.15 km^2.

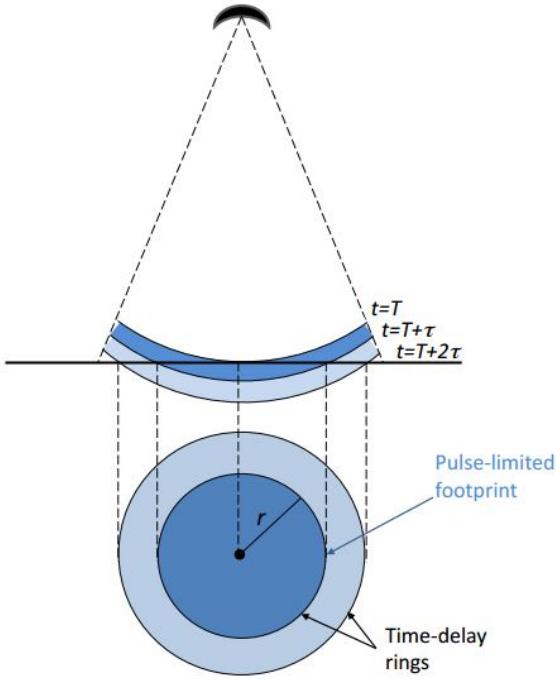

Figure 1.2: *Pulse-Limited-footprint for LRM, Source: (Footprint 2013)*

- Sharpened-Pulse-Limited footprint for SAR/SARin

  The SAR/SARin modes use a Doppler-beam-formation, which allows to discriminate the direction of the arriving echoes. Therefore, the footprint of the pulse in along-track direction can be sharpened. The width is no longer defined only by time delay, but by two independent directions: the along-track and the across-track directions, which are related to time delay. Since the Doppler-beam-formation only effects the along-track directional echoes, the across-track width of the footprint is defined by equation for pulse-limited across-track width. The width of the sharpened-pulse-limited footprint in along-track direction can be determined with:

$$\Delta x = h\frac{\lambda}{2R\nu}\,\mathrm{PRF}$$

  where

$$\begin{aligned}
&h - \text{average altitude} = 730\,\text{km}\\
&\lambda - \text{wavelength} = 0.0221\,\text{m}\\
&\nu - \text{velocity of spacecraft} = 7520\frac{\text{m}}{\text{s}}\\
&R - \text{mean Earth radius} = 6370\,\text{km}\\
&\text{PRF} - \text{Pulse Repetition Frequency} = 18.181\,\text{kHz}
\end{aligned}$$

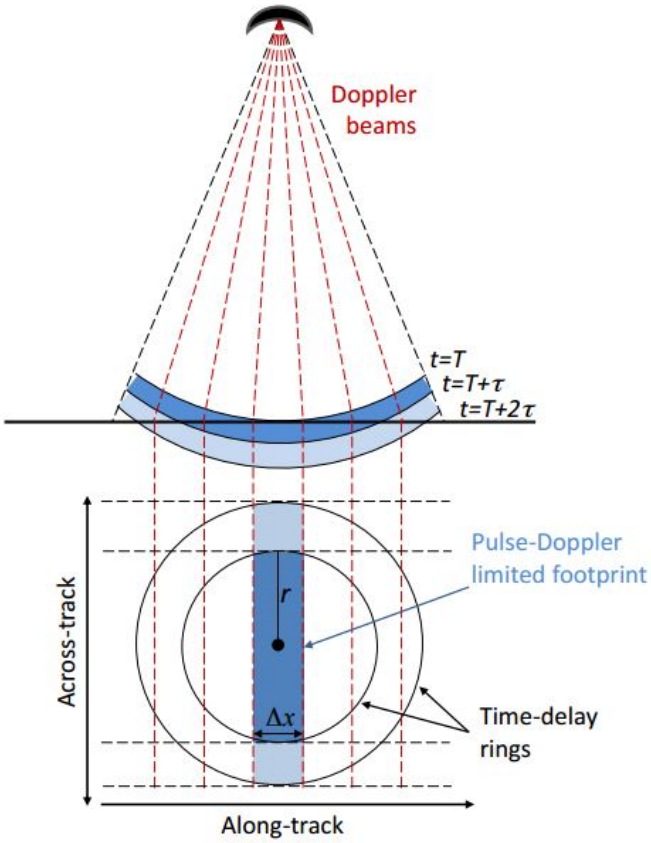

Figure 1.3: *Pulse-Doppler-limited footprint for SAR/SARin, Source: (Footprint 2013)*

These standard values yield a width in the along-track direction of approximately 305 m. Note that across-track width is significantly larger, which results in a footprint that can be approximated by a rectangular area with about 0.50 km^2.

Chapter 2

Data

2.1 CryoSat-2 Data Availability

The European Space Agency is providing all CryoSat-2 data for free on its homepage. The webapp (VisioTerra) is used to analyze the data coverage within the test terrain, see figure 2.1. The user can choose between different operation modes and specified time spans. A list of available track data is provided with direct download links.

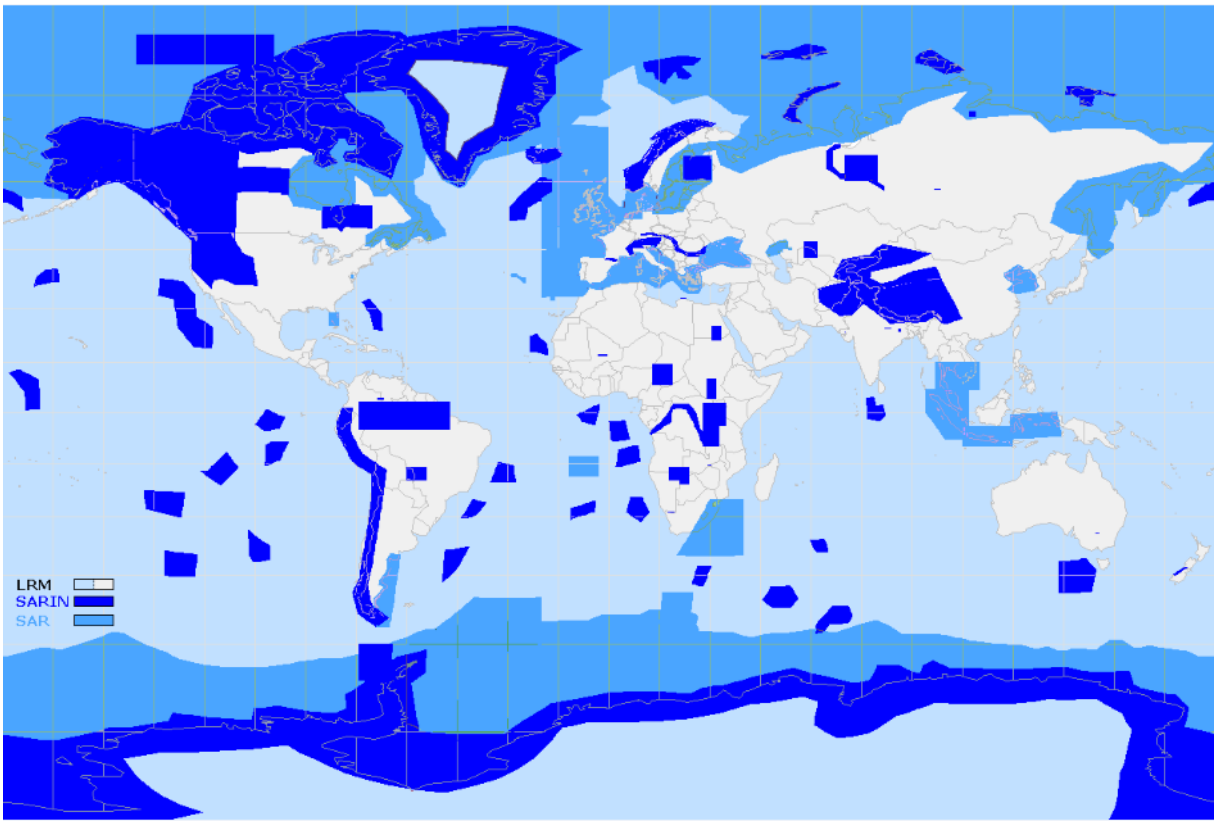

Figure 2.1: *Mode Mask, Source: (CryoSat Mode Mask)*

For the test region only SAR data is available, which comes in two different forms. First, L1b: Multi-looked Waveform Data and second L2: Elevation and other Surface Characteristics. Consequently L2-data will be used for further computations, as it consists of surface elevation and other surface parameters, such as peakiness or radar backscatter coefficient. The data is collected via pulse-limited operation with an approximate rate of 20 Hz. Although, the average datasize of one track is approximately 15 MB, an efficient computation must be written as seven years of data will be processed.

2.2 Recondition of the data

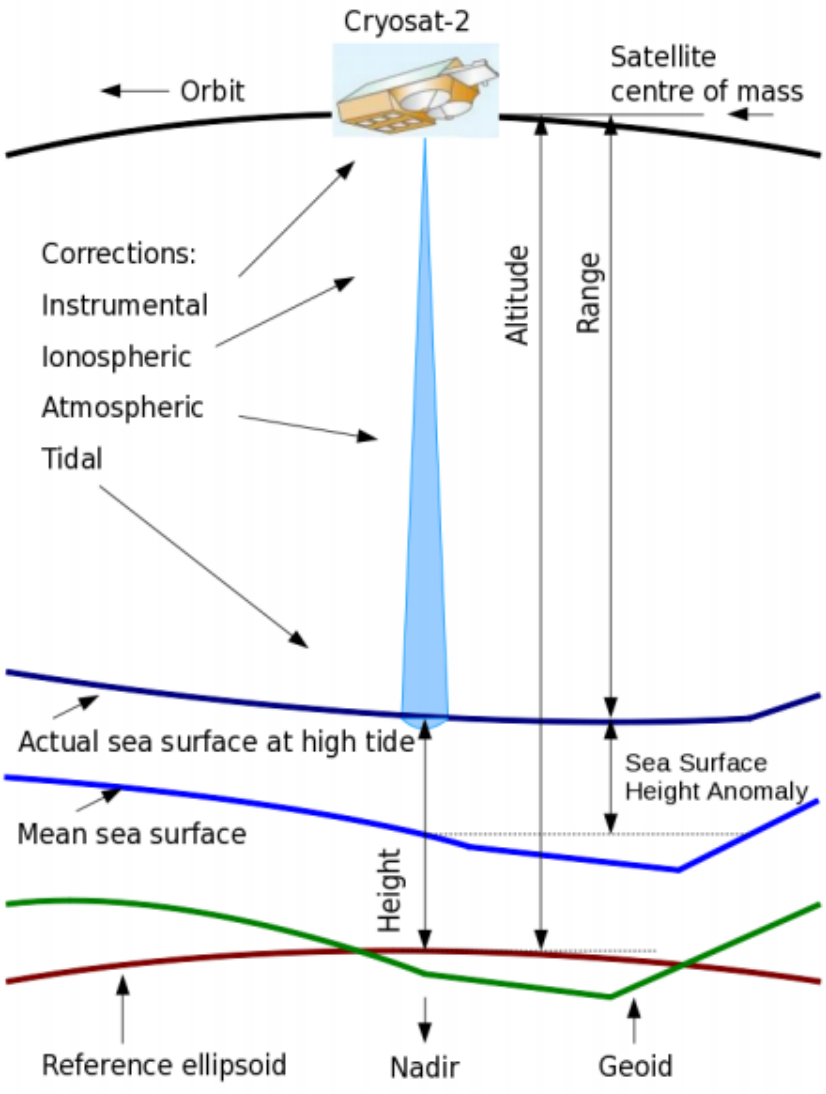

Figure 2.2: *Basic altimetry terms and functions, Source: (CS Product Handbook 2014)*

In general the satellite measures range, which is the distance between satellite and sea level. Naturally, this measurement is influenced by several disruptive factors, such as noises and errors. The errors and noises origin from different phenomenons such as barometric, atmospheric, ionospheric and tropospheric effects. In order to compensate these effects, particular corrections are applied to the range measurements, which yield sea surface height. The actual sea surface is subjected to several tidal effects such as ocean tide, ocean loading tide, solid earth tide and geocentric polar tide. These effects are summed up as the sea surface height anomaly. All of the effects contributing to the sea surface height anomaly are modelled and applied to the sea surface height measurements to yield the mean sea surface (CS Product Handbook 2014). This mean sea surface represents the geoid by form and course. Hence, the mean sea surface is the dataset of choice for further computations .

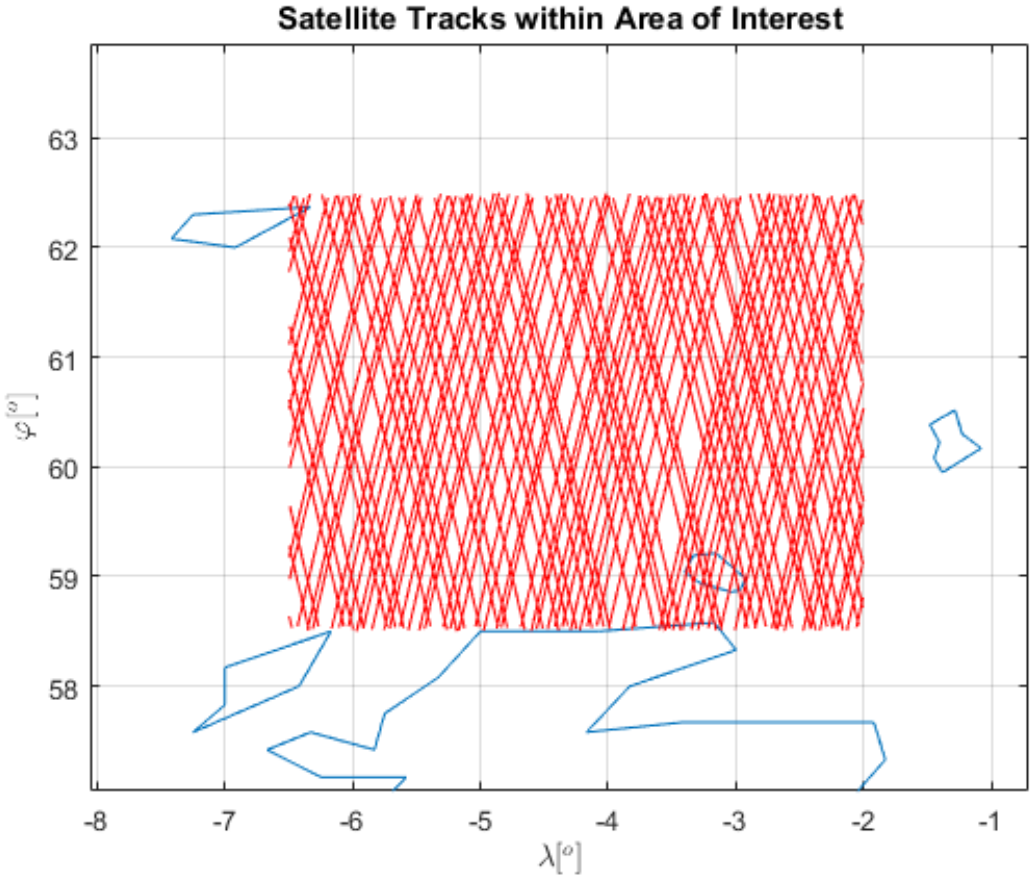

Figure 2.3: *Sample of satellite tracks within area of interest*

The figure above displays the track distribution for the chosen region. This plot visualizes tracks from only one year of data. Each line represents one track.

In virtue of the chosen method, one main component of the procedure is computation of deflections of the vertical. Given solely coordinates and geoid heights, the deflections of the vertical can only be calculated at crossover points of ascending and descending tracks. As mentioned under section 1.2 CryoSat's repeat cycle is rather long. As a result this feature provides a rather dense spacing of satellite tracks. A large amount of crossover points is

obtained through the isolated consideration of repeat tracks as separate tracks. This is possible due to the fact that repeat tracks do not match exactly their predecessor. Hence, these repeat tracks can be seen as individual tracks. As a result, an approximate amount of 1700 crossover points can be established.

2.3 FTG Data

2.3.1 Overview

The dataset used for comparison contains all Full Tensor Gradiometry components and has been collected by Bell Geospace Ltd. The area of interest has been chosen, precisely because of this dataset. The data was collected via a gradiometer mounted on a ship, crossing a nearly 60 km $\times$ 80 km area between Shetland Islands and Faroe Islands.

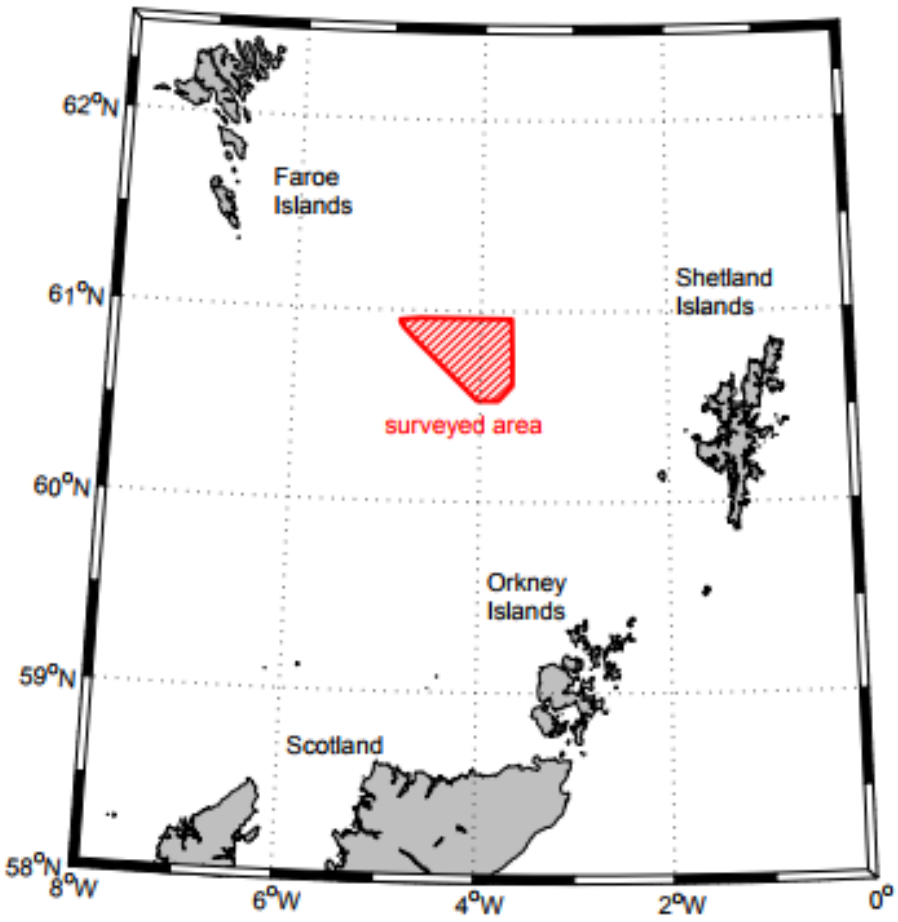

Figure 2.4: *Area surveyed by shipborne gradiometry, Source: (Roth 2009)*

2.3.2 Description and Accuracy

The gradiometric measurements were performend along trajectories across the ocean surface. According to (Roth 2009), trajectories measured in northwest-southeast direction will be called *lines* whereas northeast-southwest trajectories *ties*.

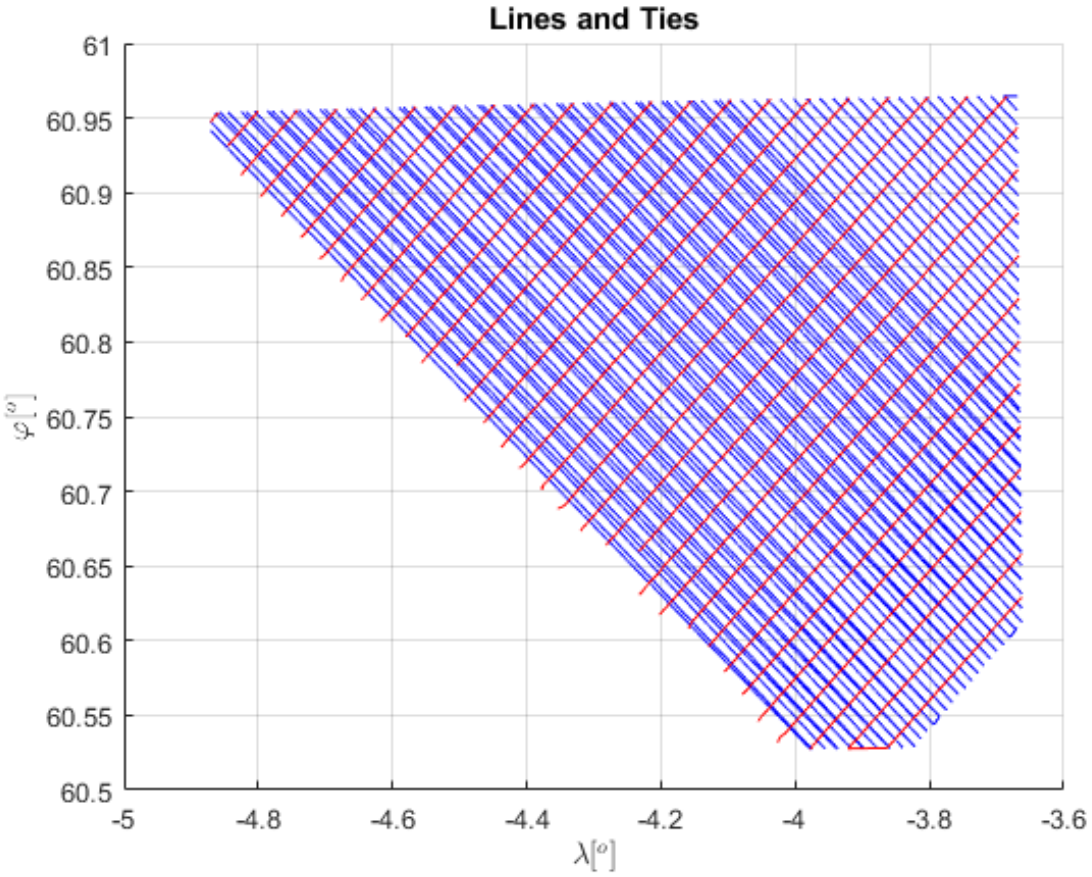

Figure 2.5: *Sample of trajectories of FTG measurements*

For every point there are several measured magnitudes:

- X_{ED50} , Y_{ED50} - Easting and Northing in datum ED50; projection of UTM zone 30 N [m]
- λ , φ - Latitude and Longitude in datum ED50 [°]
- bathy - ocean depth in sampling points [m]
- $T_{xx}, T_{xz}, T_{yx}, T_{yy}, T_{yz}, T_{zz}$ - FTG tensor components [E]
- T_{z1} - conventional gravity anomaly [mGal]
- T_{ze} - gravity anomaly derived from measured FTG data [mGal]

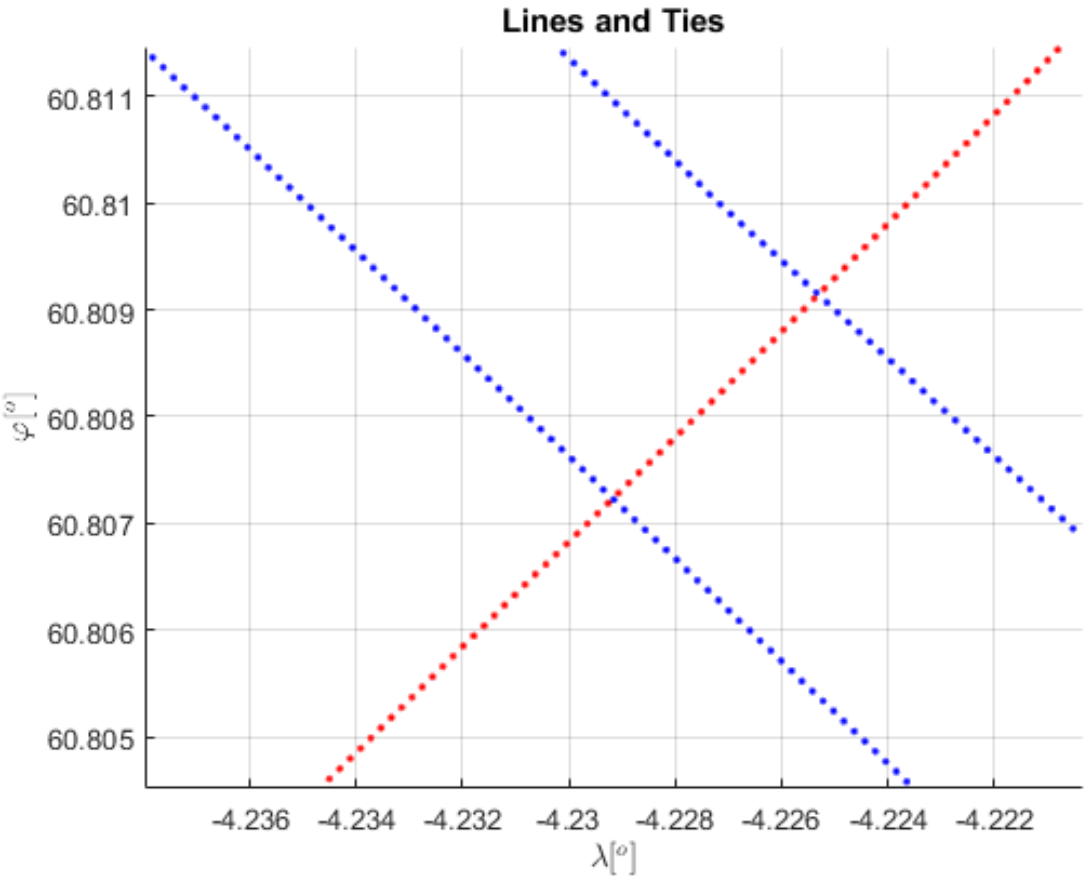

Figure 2.6: *Closeup of FTG*

The sampling distance along trajectories is approximately 15 m. While the trajectories appear as lines in figure (2.5) the closeup figure (2.6) demonstrates the sampling of the gradiometry measurements.

For every sampling point there is a $[1 \times 13]$ array in the dataset. Although, there are more than 300000 points measured in the process, the covered area is comparatively small. The spacing between the lines is about 750 m and 2250 m between ties.

Analysis of the accuracy of the gradiometric dataset has already been performed by Matthias Roth within his Bachelor Thesis in 2009. He examined the measurement data using Laplace's Equation. He reached to the conclusion, that the dataset has already been edited or filtered by its publisher Bell Geospace. For the purpose of this Bachelor Thesis it will be assumed that accuracy of the gradiometric dataset is satisfying and qualifies the measurements for further usage.
A detailed description of the procedure of investigation of accuracy can be found in Roth's Bachelor Thesis (Roth 2009).

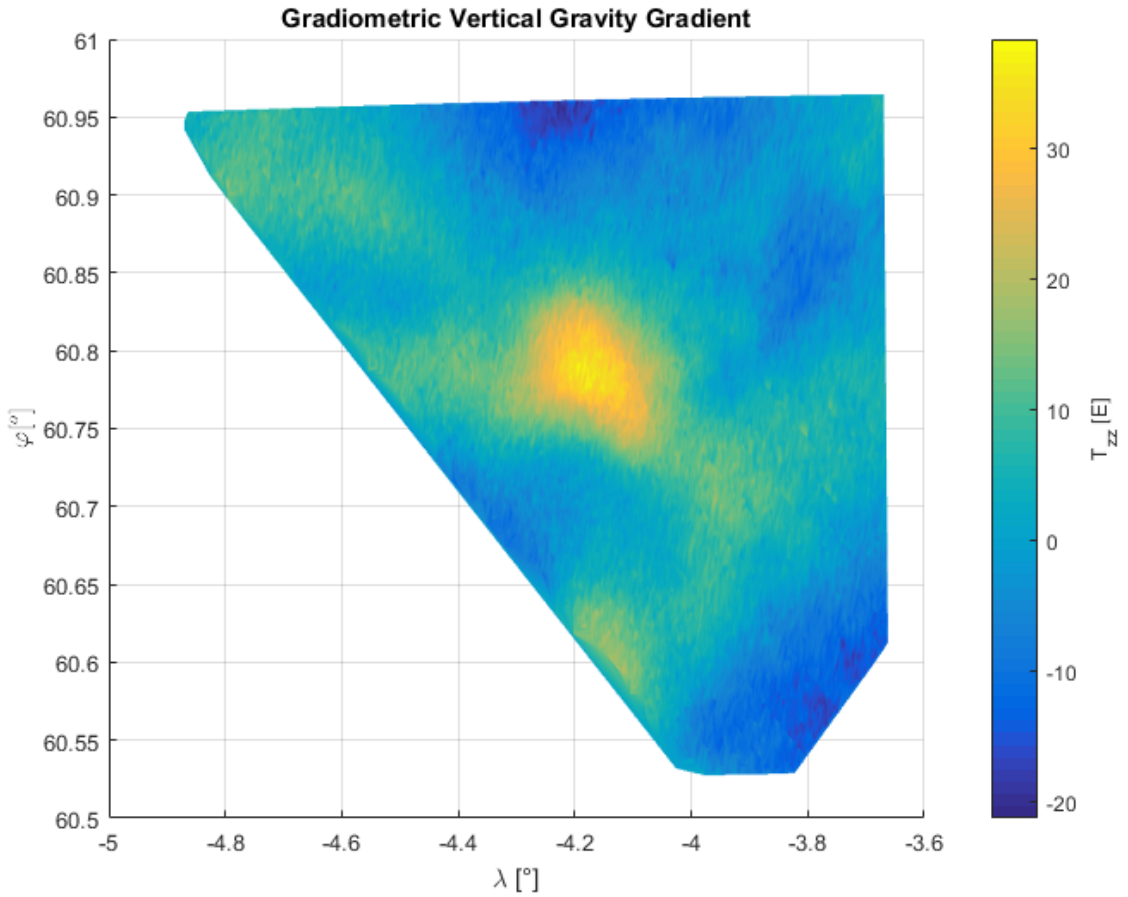

Figure 2.7: *Vertical Gravity Gradient T_{zz} from FTG*

Figure 2.7 is used to display the magnitude of the vertical gravity gradient from gradiometry in the area of interest. The most notable areas are the bulge of positive gradient values in the central region and the negative areas in the southeast region and the central northern area. Furthermore, fine structures can be observed all over the area of interest.

Chapter 3

Computations

3.1 Vertical Gravity Gradients From Deflections Of The Vertical

The ocean surface is the best natural indicator of gravity. If one hypothetically subtracts effects like wind, waves, tides and earth's rotation, the ocean will follow an equipotential surface: the Geoid. The Geoid's shape is determined by gravitational effects. One can imagine an equipotential surface as 'a surface where water does not flow', so as a surface with equal physical height. This same 'height' is the so called Potential, a magnitude of physical height. Though there is no physical height difference, i.e. equipotential, on the Geoid, there are in fact geometrical height differences of about $\pm 80\,\mathrm{m}$ compared to particular ellipsoids. These surface heights are measured by CryoSat-2 within its own reference system with respect to the WGS-84 ellipsoid. With the Geoid and the WGS-84 ellipsoid come two major magnitudes of gravitation: gravity vector and normal gravity vector. These vectors determine the direction of gravity at a certain point. The gravity vector is a plumb line with respect to the geoidal potential, whereas the normal gravity vector is a plumb line with respect to the ellipsoidal potential (normal potential). Hence, there is a difference in direction between both vectors: the deflection of the vertical. This leads to the so called gravity anomaly, which mathematically yields the gravity gradients at this certain point on the ocean surface.

In order to understand the theoretical basics of further computations one must get familiar with the phenomenon of deflection of the vertical and gravity anomaly. Although gravity anomaly will not be used in the further computations, it is nevertheless crucial to understand its nature. A point of earth's surface is projected on the reference ellipsoid by the normal vector γ, while the actual gravity vector g points towards gravity attraction. This difference is characterized by magnitude as gravity anomaly and by direction as deflection of the vertical.
Since g is defined as perpendicular to the gravitational potential surface, it points towards the actual attracting mass (Torge 1989). While γ can be calculated for every point on earth with respect to the reference ellipsoid, one only has to be concerned with the determination of the deflection of the vertical to eventually yield

$$\nabla\, \bar{g} = \nabla\, (\nabla\, T) = \begin{pmatrix} T_{xx} & T_{xy} & T_{xz} \\ T_{yx} & T_{yy} & T_{yz} \\ T_{zx} & T_{zy} & T_{zz} \end{pmatrix} \tag{3.1}$$

where the third row represents the gravity gradient

$$\nabla\, g = \begin{pmatrix} T_{zx} & T_{zy} & T_{zz} \end{pmatrix} \tag{3.2}$$

The given dataset consists of discrete points determined by longitude λ, latitude φ and geoid height N. Origin for the following computations is the relationship between geoid height N and disturbing potential T. The Bruns Formula will be used to describe this relationship

$$N = \frac{1}{\gamma} T \tag{3.3}$$

This formula can be used to determine the gravity anomaly. Bruns's Formula yields the *fundamental equation of physical geodesy* (Hofmann-Wellenhof/Moritz 2005)

$$\Delta g = -\frac{\partial T}{\partial r} + \frac{2T}{r} \tag{3.4}$$

Consideration of a flat-earth approximation leads to $r \to \infty$. Hence, the relationships

$$\frac{2T}{r} = 0 \text{ for } r \to \infty$$
$$\partial r = \partial z$$

yield the formula to determine gravity anomaly as

$$\Delta g = -\frac{\partial T}{\partial z} \tag{3.5}$$

$$\frac{\partial \Delta g}{\partial z} = -\frac{\partial^2 T}{\partial z^2} \tag{3.6}$$

The local coordinate system is defined as a left-handed xyz-system. The x-axis is pointing towards north as a meridian. The z-axis is perpendicular to the x-axis and orthogonal to the surface. The y-axis complements the system to a left-handed system.

The north-component of deflection of the vertical is the slope of the geoid in x direction and therefore can be described by derivation with respect to x as

$$\xi(\mathbf{x}) = -\frac{\partial N}{\partial x} = -\frac{1}{\gamma}\frac{\partial T}{\partial x} \tag{3.7}$$

The east-component of deflection of the vertical is the slope of the geoid in y direction and therefore can be described by derivation with respect to y as

$$\eta(\mathbf{y}) = -\frac{\partial N}{\partial y} = -\frac{1}{\gamma}\frac{\partial T}{\partial y} \tag{3.8}$$

One uses Laplace's equation with the former determined relations to eventually yield vertical gravity gradients.

$$\frac{\partial^2 T}{\partial x^2} + \frac{\partial^2 T}{\partial y^2} + \frac{\partial^2 T}{\partial z^2} = 0 \tag{3.9}$$

Modification of formulas (3) and (4) indicate that the sum of the x derivative of east-component and y derivative of north-component ξ yield the vertical gravity gradient as it is determined as the z derivative of gravity anomaly:

$$\frac{\partial \Delta g}{\partial z} = -\gamma \left(\frac{\partial \eta}{\partial x} + \frac{\partial \xi}{\partial y} \right) \tag{3.10}$$

As the basic concept is established it will be further tried to resolve these calculations with numeric data. Main task is to compute components of vertical deflection. Regarding the available data, the most suitable method is starting with the formula of Vening-Meinesz (Heiskanen/Moritz 1981)

$$\eta = -\frac{1}{R \cos \varphi} \frac{\partial N}{\partial \lambda} \tag{3.11}$$

$$\xi = -\frac{1}{R} \frac{\partial N}{\partial \varphi} \tag{3.12}$$

This formula connects η and ξ with geodetic coordinates λ and φ. Next, these derivations of geoid height N will be examined with respect to time along ascending and descending profiles (Sandwell 1992)

$$\dot{N}_\mathrm{a} = \frac{dN_\mathrm{a}}{dt} = \frac{\partial N}{\partial \lambda} \dot{\lambda}_\mathrm{a} + \frac{\partial N}{\partial \varphi} \dot{\varphi}_\mathrm{a} \tag{3.13}$$

$$\dot{N}_\mathrm{d} = \frac{dN_\mathrm{d}}{dt} = \frac{\partial N}{\partial \lambda} \dot{\lambda}_\mathrm{d} + \frac{\partial N}{\partial \varphi} \dot{\varphi}_\mathrm{d} \tag{3.14}$$

It is important to distinguish between orbit direction (ascending or descending), as it will be of use later while modifying equations 3.21 and 3.22. Given the altimetry data one must use numeric differentiation to calculate these derivations:

$$\dot{N}_\mathrm{a} = \frac{dN_\mathrm{a}}{\partial t} = \frac{N_\mathrm{a}(t + \Delta t) - N_\mathrm{a}(t - \Delta t)}{2\Delta t} \tag{3.15}$$

$$\dot{N}_\mathrm{d} = \frac{dN_\mathrm{d}}{\partial t} = \frac{N_\mathrm{d}(t + \Delta t) - N_\mathrm{d}(t - \Delta t)}{2\Delta t} \tag{3.16}$$

The functions $\dot{\lambda}$ and $\dot{\varphi}$ are the longitudinal and latitudinal components of the satellite's ground track velocity. Regarding the nearly circular orbit of CryoSat-2, its velocity mainly depends on latitude. Analyzation of the accuracies of the following relationships between ascending and descending ground track velocities at the crossover points can be found in Appendix A.

$$\dot{\lambda}_\mathrm{a} = \dot{\lambda}_\mathrm{d} \tag{3.17}$$

$$\dot{\varphi}_\mathrm{a} = -\dot{\varphi}_\mathrm{d} \tag{3.18}$$

The coordinates of crossover points are geodetic coordinates. Consequently, latitudinal velocity is mainly influenced by earth's oblateness. Equatorial bulges will accelerate or decelerate the satellite in its latitudinal velocity. Longitudinal velocity depends not only on latitude,

but also on earth's rotation around its spin axis and the nodal precession of the satellite orbit. (Sandwell 1992)

$$\dot{\lambda} = \omega_s \frac{\cos I}{\cos^2 \phi} - (\omega_e - \omega_n) \tag{3.19}$$

$$\dot{\varphi} = \omega_s \sqrt{1 - \frac{\cos^2 I}{\cos^2 \phi}} \tag{3.20}$$

with

$$\begin{aligned} \omega_{\mathrm{s}} &- \text{satellite orbit frequency} && \left[\frac{\mathrm{rad}}{\mathrm{s}}\right] \\ \omega_{\mathrm{e}} &- \text{earth rotation frequency} && \left[\frac{\mathrm{rad}}{\mathrm{s}}\right] \\ \dot{\Omega}_{\mathrm{n}} &- \text{nodal precession frequency} && \left[\frac{\mathrm{rad}}{\mathrm{s}}\right] \\ I &- \text{satellite orbit inclination} && [\mathrm{rad}] \end{aligned}$$

Applying the above relations will guarantuee accurate velocities for further computations. Using (3.19) and (3.20) to modify (3.15) and (3.16) will eventually yield the geoid gradient

$$\frac{\partial N}{\partial \lambda} = \frac{1}{2\dot{\lambda}} (\dot{N}_{\mathrm{a}} + \dot{N}_{\mathrm{d}}) \tag{3.21}$$

$$\frac{\partial N}{\partial \varphi} = \frac{1}{2|\dot{\varphi}|} (\dot{N}_{\mathrm{a}} - \dot{N}_{\mathrm{d}}) \tag{3.22}$$

As geodetic coordinates are given and used, utilization of Bruns's formula and Laplace's Equation has to be in geodetic coordinates, too. The derivation was established by Vening-Meinesz in (Heiskanen/Moritz 1981). The vertical gravity gradient is given from differentiation $\frac{\partial}{\partial r}$ of (3.4) as

$$\frac{\partial \Delta g}{\partial r} = \frac{\partial^2 T}{\partial r^2} + \frac{2}{r}\frac{\partial T}{\partial r} - \frac{2}{r^2} T \tag{3.23}$$

Regarding Laplace's equation $\Delta T = 0$ in spherical coordinates

$$\frac{\partial^2 T}{\partial r^2} + \frac{2}{r}\frac{\partial T}{\partial r} - \frac{\tan \varphi}{r^2}\frac{\partial T}{\partial \varphi} + \frac{1}{r^2}\frac{\partial^2 T}{\partial \varphi^2} + \frac{1}{r^2 \cos^2 \varphi}\frac{\partial^2 T}{\partial \lambda^2} = 0 \tag{3.24}$$

Through combination of both formulas above and a constant radius approximation $r = R$, one is able to yield the expression for the vertical gravity gradient as

$$\frac{\partial \Delta g}{\partial r} = \frac{2}{R^2} T - \frac{\tan \varphi}{R^2}\frac{\partial T}{\partial \varphi} + \frac{1}{R^2}\frac{\partial^2 T}{\partial \varphi^2} + \frac{1}{R^2 \cos^2 \varphi}\frac{\partial^2 T}{\partial \lambda^2} \tag{3.25}$$

Using Bruns's formula $T = \gamma N$ one obtains

$$\frac{\partial \Delta g}{\partial r} = \frac{2\gamma}{R^2} N - \frac{\gamma}{R^2} \tan \varphi \frac{\partial N}{\partial \varphi} + \frac{\gamma}{R^2}\frac{\partial^2 N}{\partial \varphi^2} + \frac{\gamma}{R^2 \cos^2 \varphi}\frac{\partial^2 N}{\partial \lambda^2} \tag{3.26}$$

Regarding the components of deflection of the vertical these will now be used to substitute the second derivatives of geoid height

$$\frac{\partial N}{\partial \varphi} = -R\xi \qquad \rightarrow \frac{\partial^2 N}{\partial \varphi^2} = -R\frac{\partial \xi}{\partial \varphi} \tag{3.27}$$

$$\frac{\partial N}{\partial \lambda} = -R\cos\varphi\,\eta \qquad \rightarrow \frac{\partial^2 N}{\partial \lambda^2} = -R\cos\varphi\frac{\partial \eta}{\partial \lambda} \tag{3.28}$$

The derivations of deflections of the vertical will be performed as numerical differentiation. Since the distances between crossover points can reach up to several kilometers it is important to define an algorithm for proper computation. First, the deflections of the vertical ξ, η will be interpolated onto the Full Tensor Gradiometry data points. With an along-track spacing of approximatley 15 m between each FTG point it is possible to perform numerical differentiation of ξ with respect to φ and η with respect to λ.

Eventually vertical gravity gradients will be determined by

$$\frac{\partial \Delta g}{\partial r} = \frac{2\gamma}{R^2}N + \frac{\gamma}{R}\tan\varphi\,\xi + \frac{\gamma}{R}\frac{\partial \xi}{\partial \varphi} + \frac{\gamma}{R\cos\varphi}\frac{\partial \eta}{\partial \lambda} \tag{3.29}$$

With

$$Rd\varphi = dx \qquad R\cos\varphi d\lambda = dy \tag{3.30}$$

it is possible to establish the relation with Equation (3.10).

3.2 Interpolation

The following step is to interpolate vertical gravity gradients from altimetric data onto the points of gradiometric measurements. This way an actual comparison can be generated.

3.2.1 Point Distribution

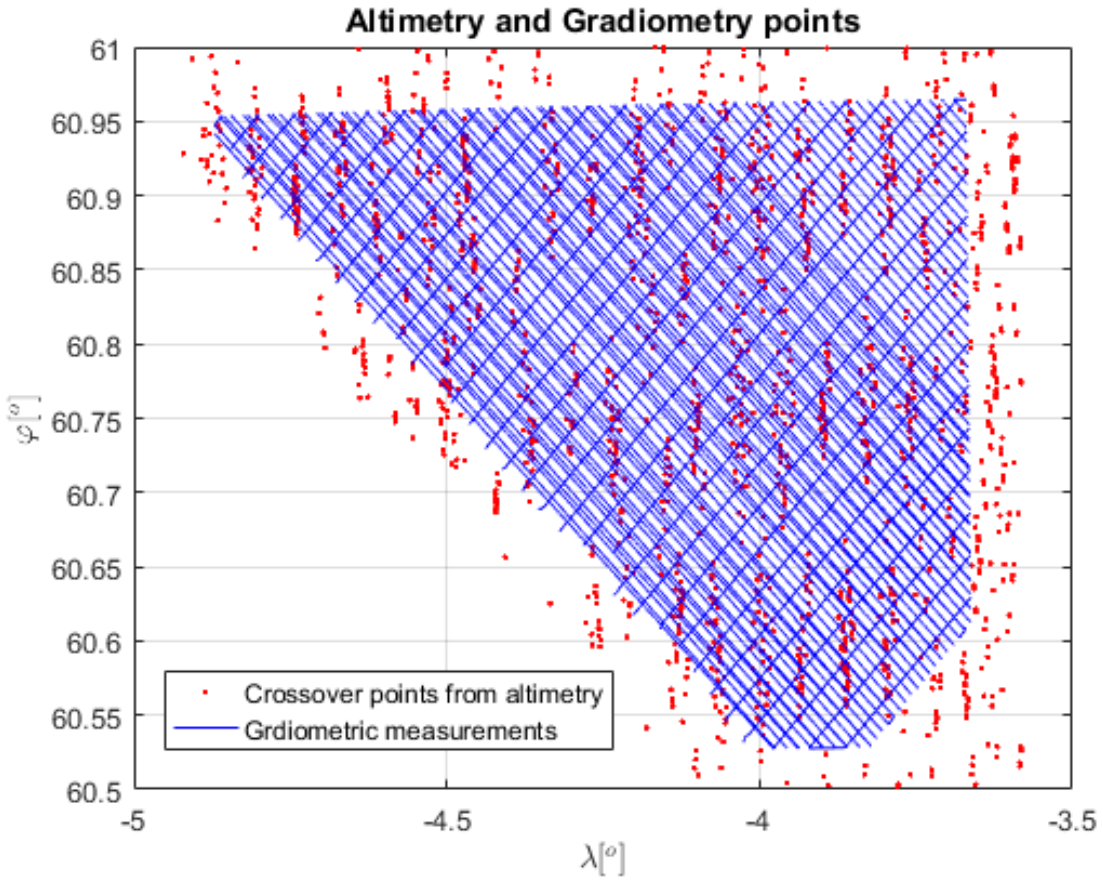

Figure 3.1: *Distribution of altimetric crossover points and FTG-points*

The challenge of interpolating altimetric data onto gradiometric data is that there is simply no information available in the rather large gaps of the altimetric dataset compared to the gradiometric one.
As displayed in figure 3.1, the distribution of altimetric points is rather arbitrary compared to the frequent patterns of gradiometric data. Furthermore, the crossover points gather in clusters due to repeat orbit pattern.

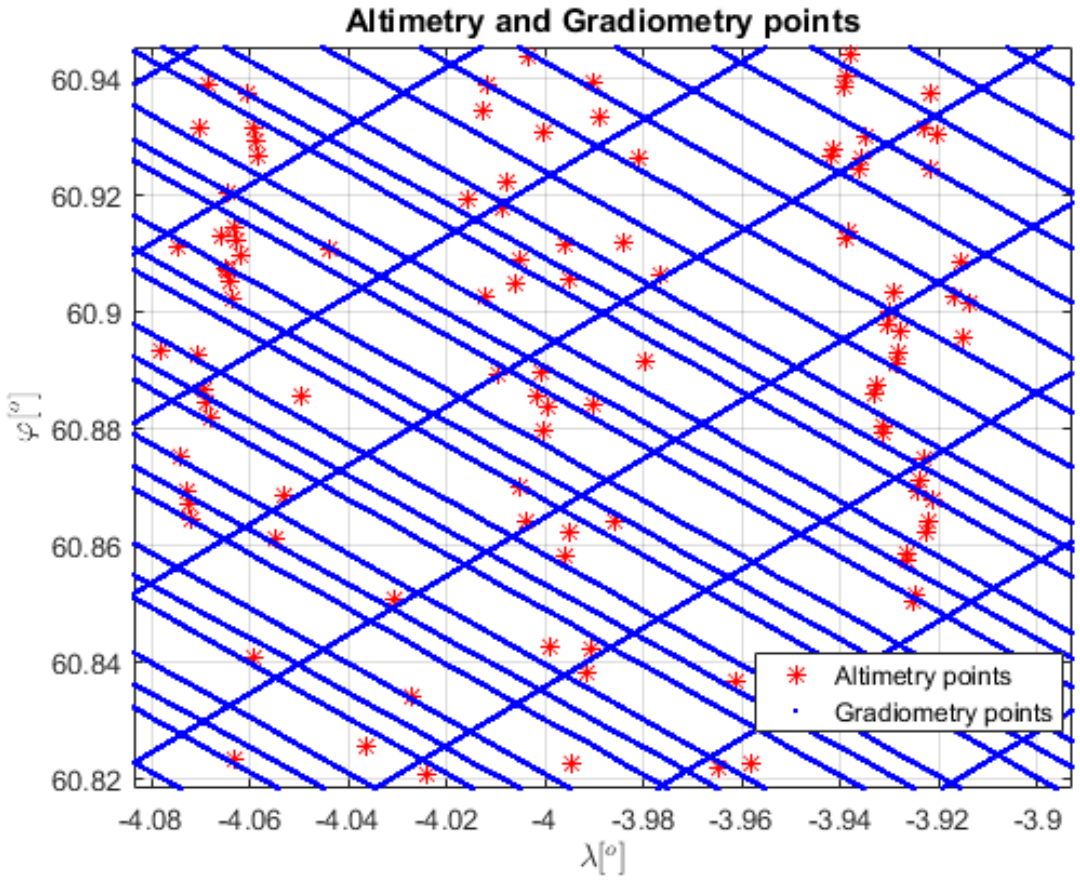

Figure 3.2: *Favourable Crossover Point Distribution*

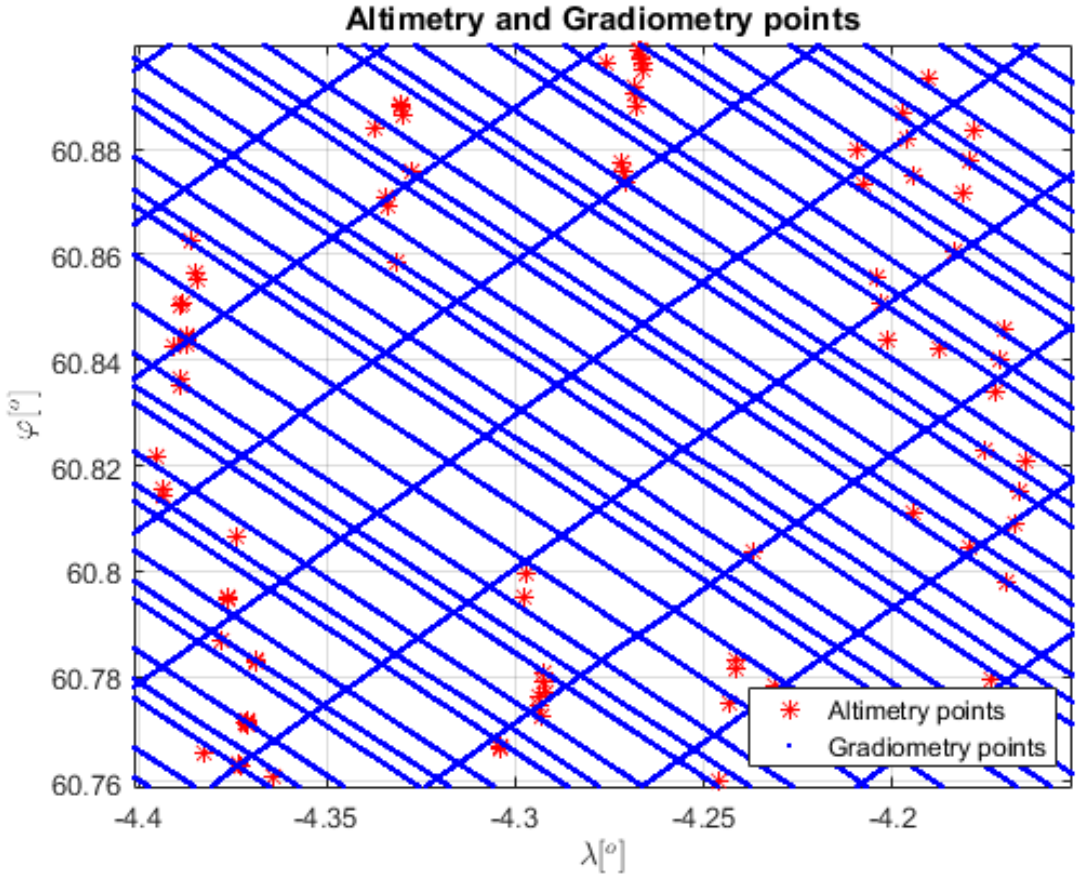

Figure 3.3: *Unfavourable Crossover Point Distribution*

In the case of figure 3.2 the influence of this behaviour is not crucial. However, regarding figure 3.3 one is forced to take care of this delicate problem within interpolation.

The choice of the interpolation method is of utter importance. The default interpolation scheme of matlab is baseributiod on triangle interpolation method, (Zhao 2012). As the altimetric dataset provides only few points, one is compelled to find a more effective and particularly accurate interpolation method. Moreover, investigation among interpolation onto seperate grid has proven inaccurate. The rather fine structures of T_{zz} information can not be reproduced or approached. The process to yield suitable results is called *Inverse Distance Weighting Interpolation*. This interpolation method does not use a triangulation approach and is free from a particular grid.

3.2.2 Inverse Distance Weighting Interpolation

Using Inverse Distance Weighting Interpolation provides the possibility to interpolate a discrete scattered set of points onto a grid or an other set of points. In order to assign a value to an unknown point, all the values of known points within a certain radius will be used. The weighting of a known value depends on the distance between measured and the interpolated point. The closer the measured value is, the bigger the weighting is. To determine the gravity gradient values for a given point based on samples, the following formula will be used:

$$u_j = \frac{\sum_{i=1}^{N} w_{ij} u_i}{\sum_{i=1}^{N} w_{ij}} \tag{3.31}$$

where variables denote as

u_i - known gravity gradient value
u - interpolated value
N - number of known points
ω_i - weights

Computation of ω is implemented as

$$\omega_i = \frac{1}{d_{x,x_i}^p} \tag{3.32}$$

with

d_{x,x_i} - distance between known point x_i and point of interest x
p - power

A satisfying interpolation depends on two factors

- Search Radius
  Regarding the sparse distribution of altimetry data, the determination of the search radius is crucial. Points of interest need several points of value to ensure an extensive determination of the value. As there is an across-track FTG-points every 15 m, a small radius would be sufficient. However, the spacing between altimetry data points can reach up to some kilometers. A large radius will increase the processing time seriously. It

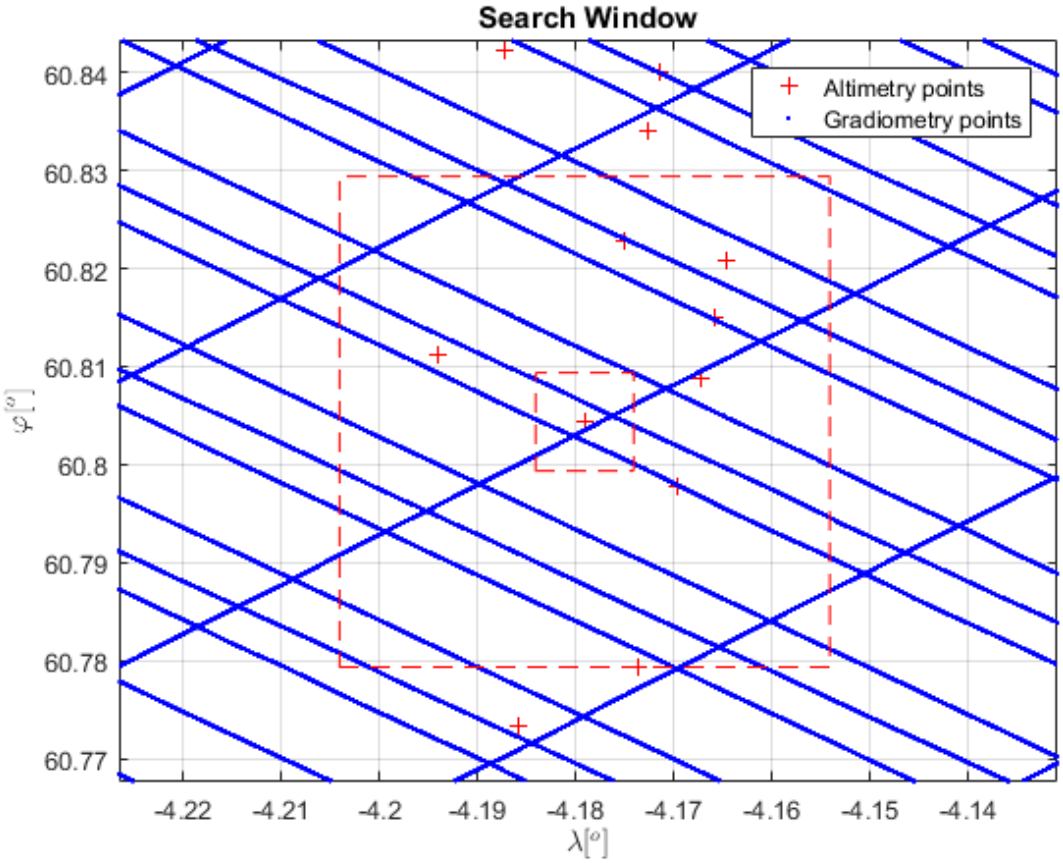

Figure 3.4: *Search window: Small with box edge* 0.01 ° *, large with box edge* 0.05 °

appears that the spacing between discrete points of measurement is so dense that tracks appear as lines in 3.4. With approximately 300000 points the FTG-dataset provides a large amount of measurements for interpolation. However, one has to consider the interpolation algorithm regarding computation time.

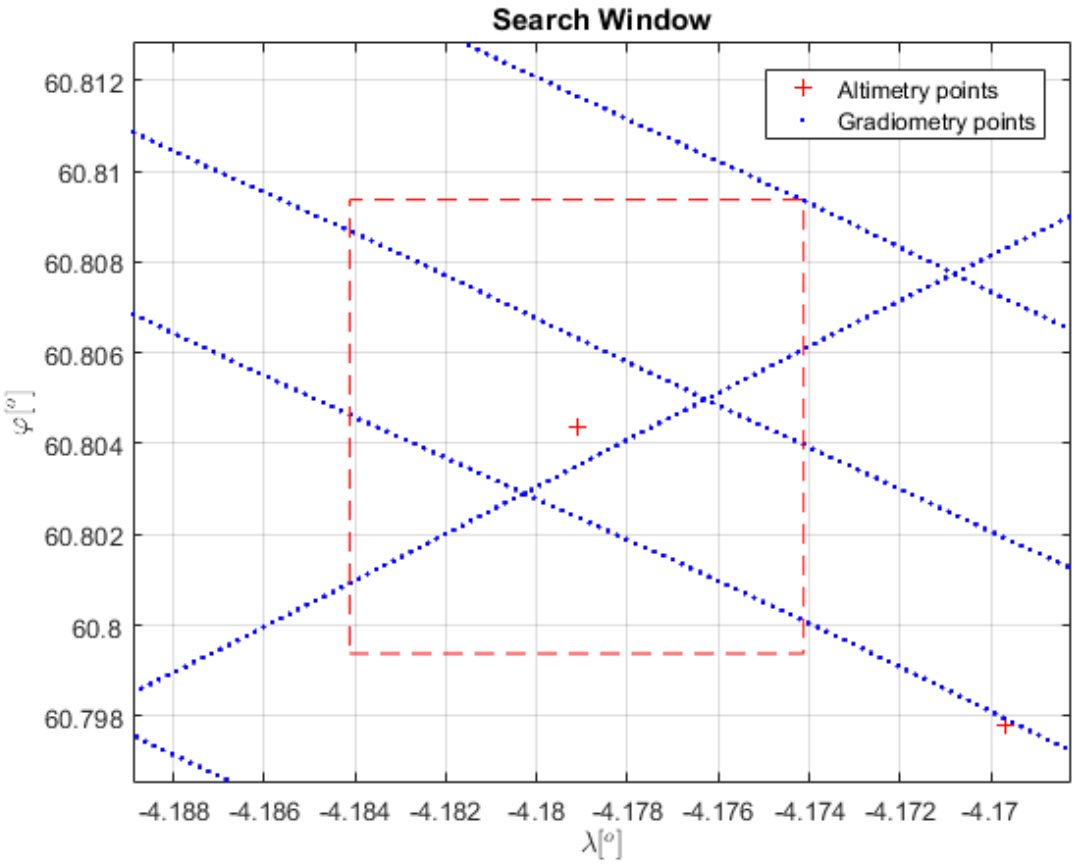

Figure 3.5: *Closeup of Search Window area with box edge* 0.01 °

Moreover, spacing between altimetry points is rather large especially in areas such as in 3.3. Choosing a wide radius leads to contribution of distant values which might not relate to the point of interest.
In order to reduce computation time a search window with the form of a box has been chosen. The algorithm examines longitude and latitude of interpolation points. Only points within this box window will be used for interpolation. Furthermore, a minimum amount of points contributing to the interpolated value is required. If this minimum condition is not fulfilled, the size of the box edges will be increased.

- Weighting
  The weighting depends on the particular distance between the known and the unknown points. Since the distance is set as denominator the weighting will rise extremely for close points, yielding an enormous interpolated value.

The algorithm will search for all FTG-points within a ceartain radius surrounding the value point, i.e. a crossover point. For each point within this radius a value will be interpolated. After a complete interpolation iteration the algorithm increases the radius in order to reach points unaffected by the former iteration.

3.3 Comparison

Eventually, the interpolated vertical gravity gradients will be compared to the gradiometric T_{zz} elements. First, one must provide an overview of the differences between interpolated and measured values. An ideal tool to represent the differences is the histogram.

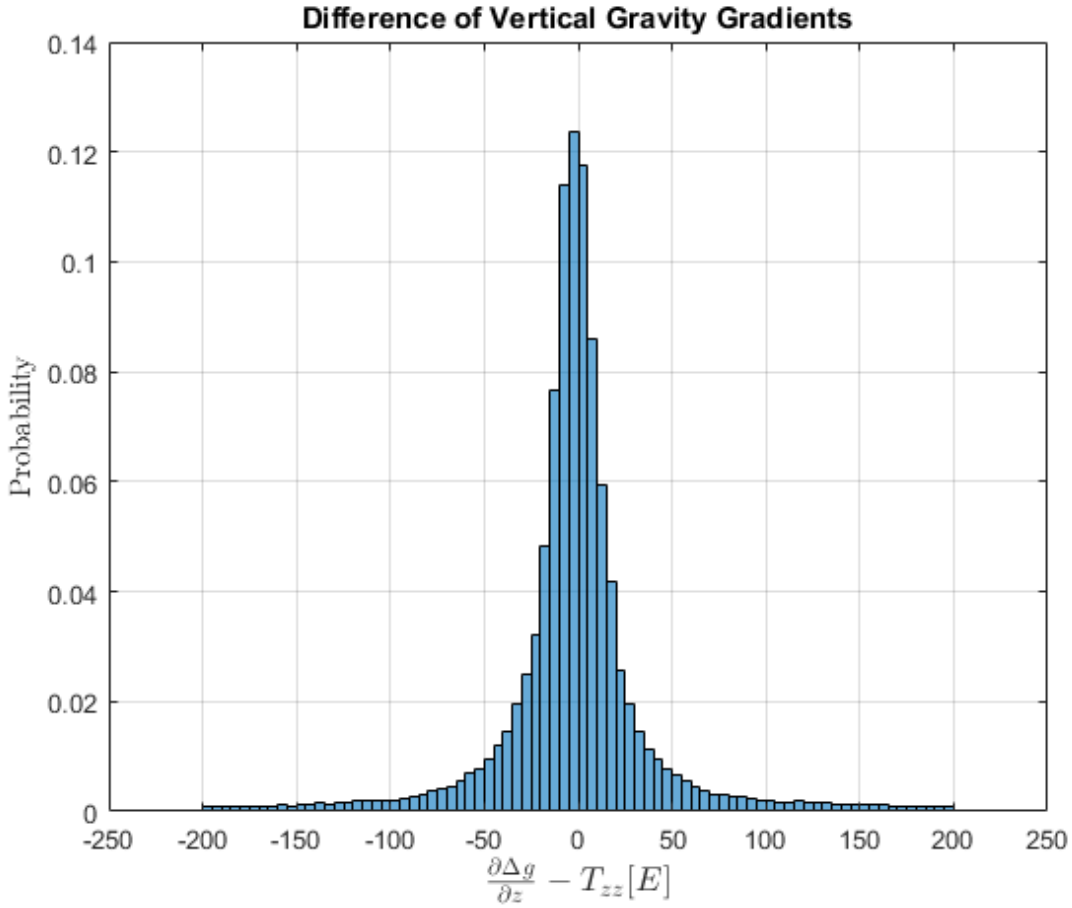

Figure 3.6: *Histogram of* $\frac{\partial \Delta g}{\partial z} - T_{zz}$

Figure 3.6 displays the difference between interpolated vertical gravity gradients from altimetry and measured vertical gravity gradients from gradiometry. The histogram indicates a Gaussian distribution. However, the interval is extremely widespread reaching from differences beyond $-200\,\mathrm{E}$ to far above $200\,\mathrm{E}$. Regarding the proportion of these extreme values one may indicate them as outliers. Still, the graph implies great differences between interpolated values and measured values. The statistic parameters for this difference field are

$$\sigma_{\mathrm{Diff}} = 13.182\,\mathrm{E} \qquad \mu_{\mathrm{Diff}} = -1.698\,\mathrm{E}$$

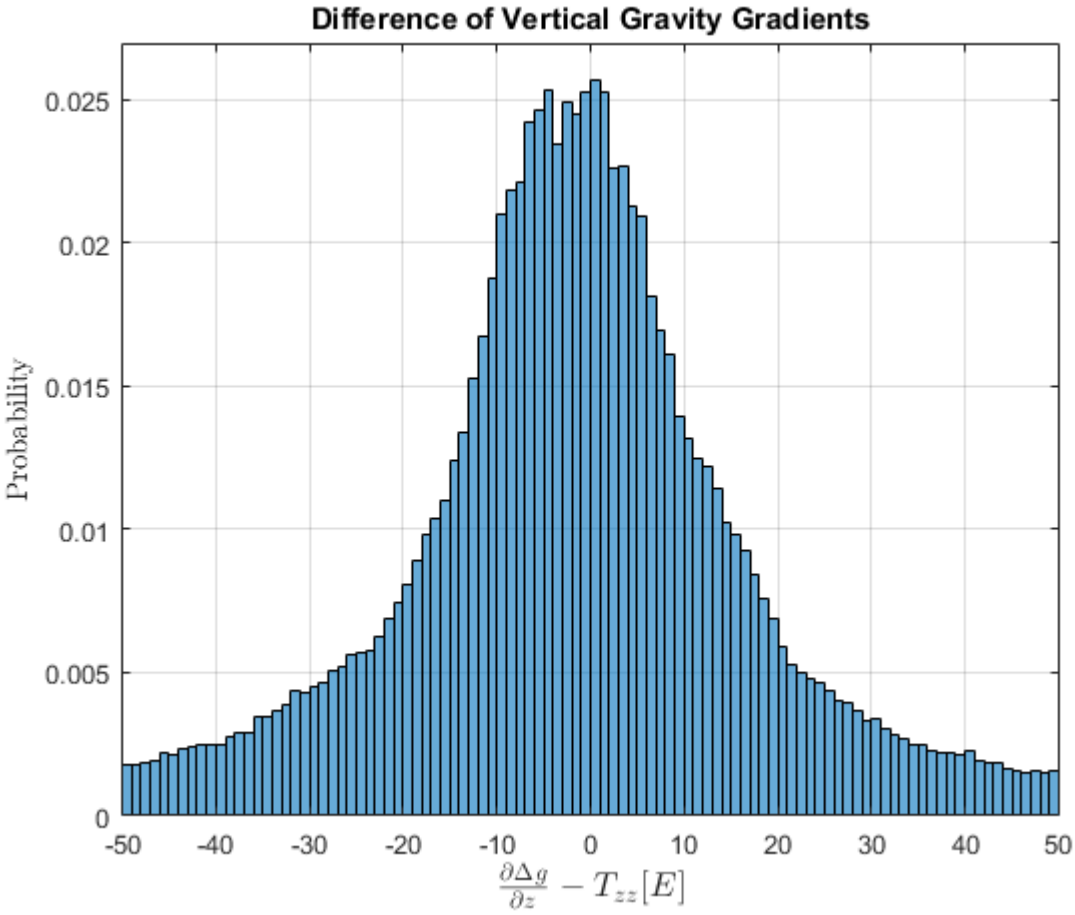

Figure 3.7: *Closeup of Histogram in figure 3.6*

Generating deflections of the vertical uses first degree derivations of ground track positions and geoid heights. The deflections of the vertical in turn will be differentietad with respect to λ and φ to yield the vertical gravity gradient. These derivations tend to magnify slight variations in deflection of the vertical data into large discontinuities. Moreover, the crossover data used for interpolation is given in clusters in certain areas. Particular remote regions of the testfield demand a large interpolation radius. Consequently, crossover points which technically barely affect the interpolated value in these remote points contribute to the vertical gravity gradient.

Comparing statistic parameters σ and μ of both datasets

$$\begin{aligned} \sigma_{\text{FTG}} &= 3.005\,\text{E} & \mu_{\text{FTG}} &= 2.612\,\text{E} \\ \sigma_{\text{Interpolation}} &= 13.168\,\text{E} & \mu_{\text{Interpolation}} &= 0.913\,\text{E} \end{aligned}$$

The standard deviation of the interpolated dataset exceeds the standard deviation of the measured dataset by far. The interpolated vertical gravity gradients are extremely scattered. Furthermore, the mean value of interpolated vertical gravity gradients is closer to zero.

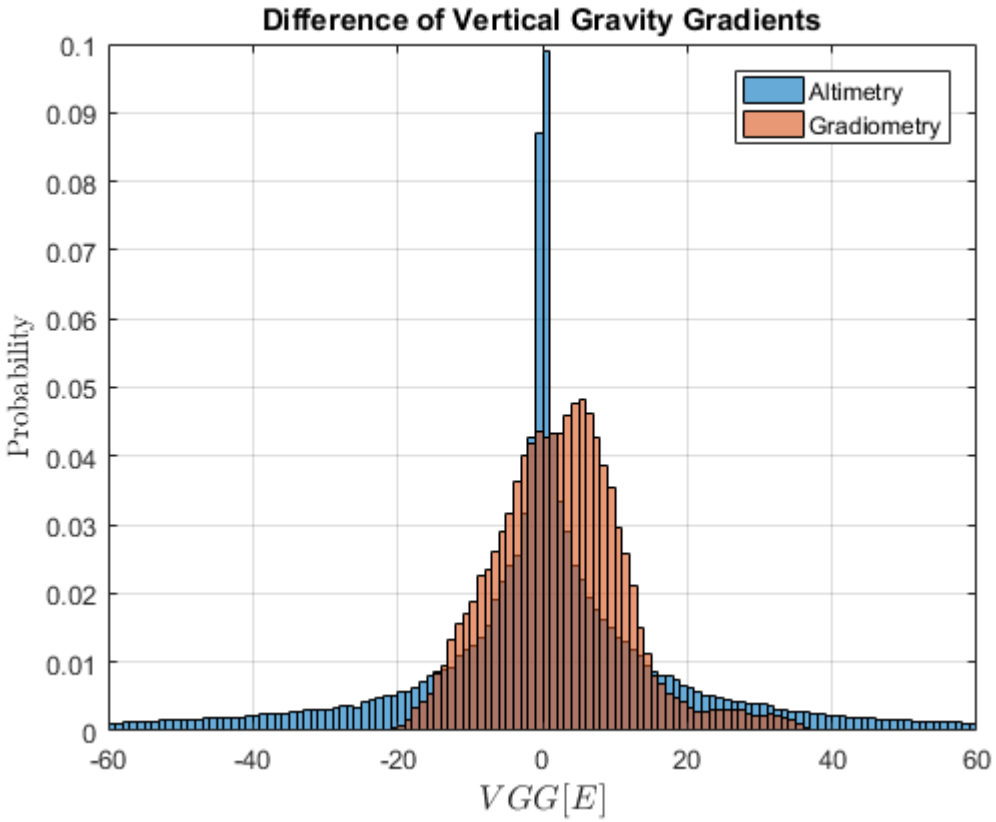

Figure 3.8: *Histograms for altimetric and gradiometric vertical gravity gradients*

Also a large amount of interpolated values is close to zero. Distant points contributing to an interpolated value assign a minor weighting and therefore surpass the algorithm for minimum contributing points.

For exemplaric analysis the interpolated dataset will be edited beforehand. Points with differences between vertical gravity gradients exceeding 10 E will be neglected. Additionally, points with an interpolated value virtually zero will not be taken into consideration.

The statistic parameters after rejection of outliers are

$$\sigma_{\text{Diff}} = 5.422\,\text{E} \qquad \mu_{\text{Diff}} = -0.564\,\text{E}$$

3.3.1 Exemplaric Analysis

In this section particular Lines with diverse point density will be analyzed. Items of analyzation are point density and its impact on magnitude of differences, continuity of datasets and smoothness of along track course. The lines chosen are line 56 and line 68. The characteristics about line 68, that it crosses the entire expansion of the test region and additionally contain almost thoroughly interpolated areas in it south-eastern course. The second line of investigation, line 56 does pass the large interpolation gap in the center of the test region. Item of ivestigation will be the behaviour of the values in this particular area.

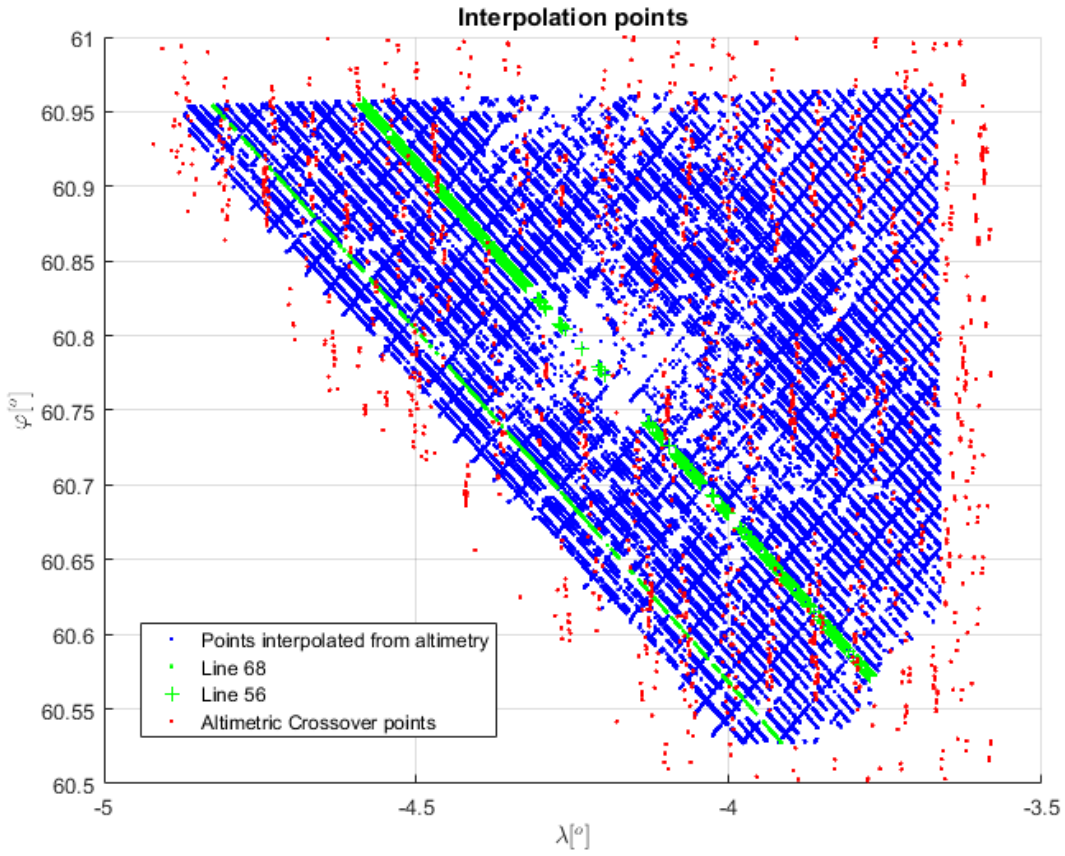

Figure 3.9: *Lines 56 and 68 in the Difference Field*

Figure 3.10 displays the course of interpolated and measured vertical gravity gradients with respect to distance along the track. The graph proves the resemblence between both datasets. Interpolated values comply the gradiometric data. However, interpolation values turn out as more volatile than the measured gradients. The interpolated points within this line reach a RMS of 5.485 E.

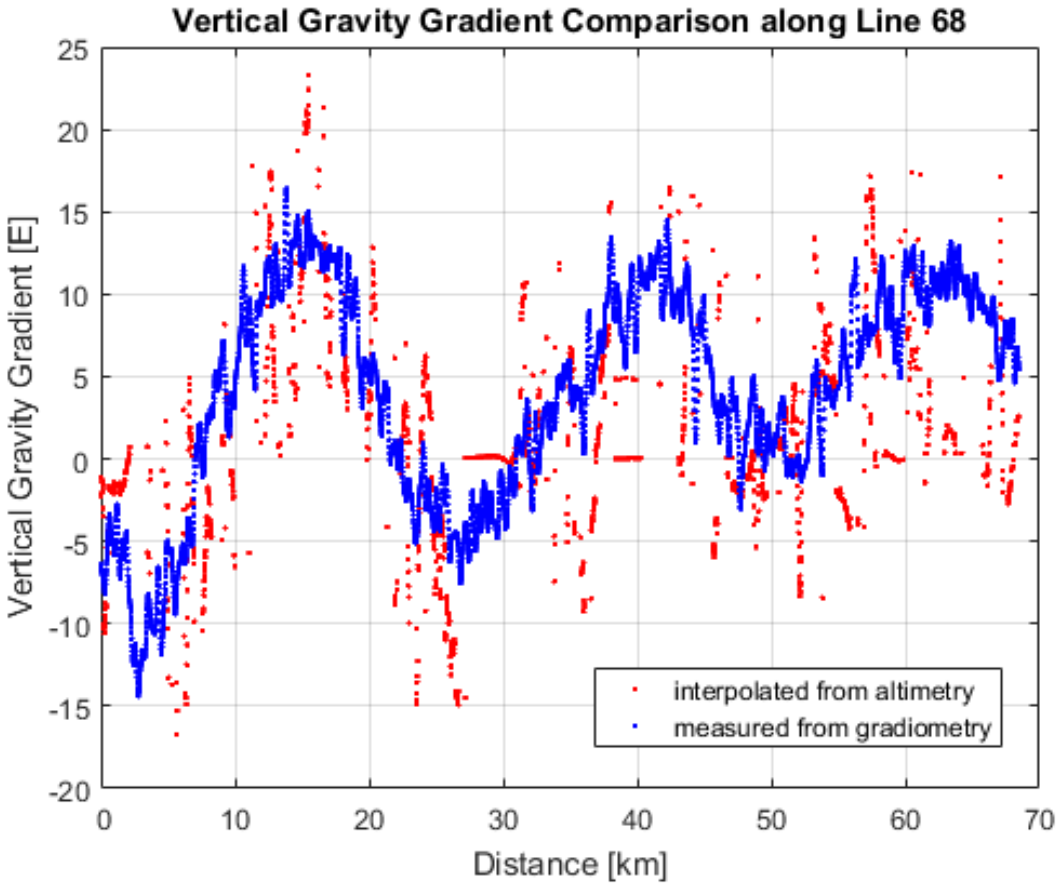

Figure 3.10: *Along track course of Line 68*

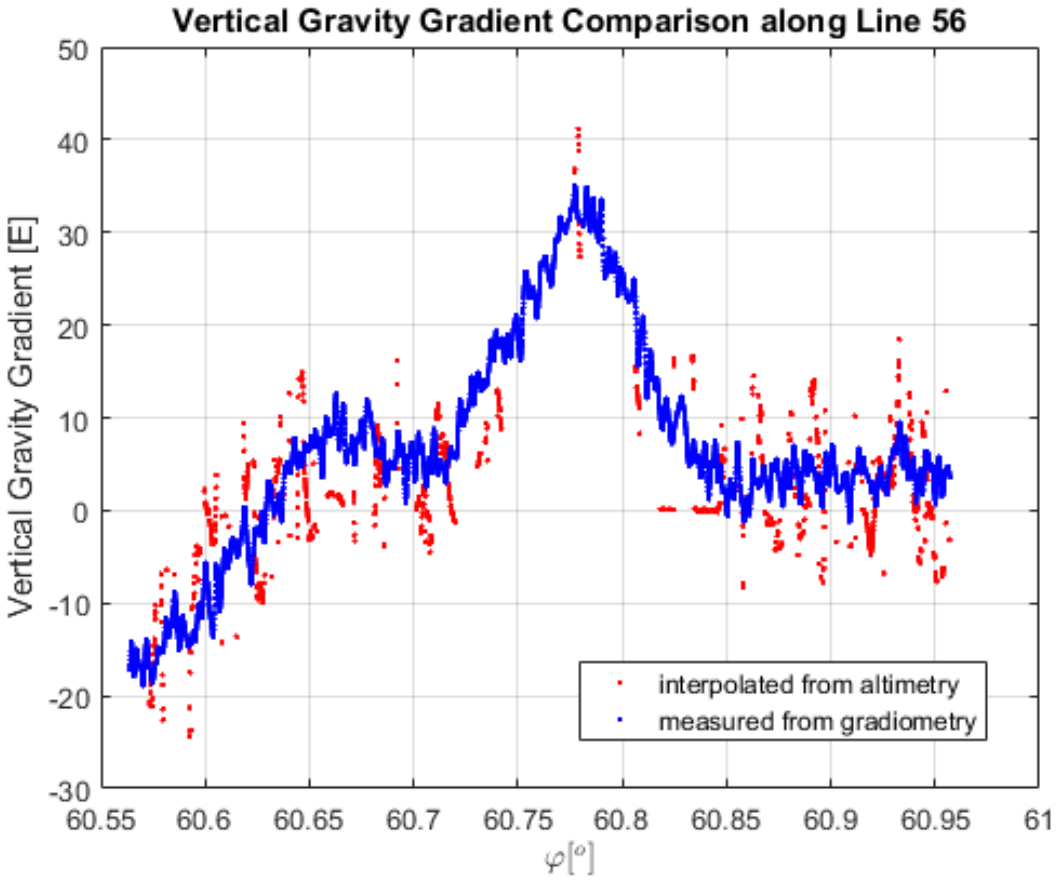

Figure 3.11: *Course of Line 56 with respect to Latitude*

The graph in figure 3.11 of interpolated values resembles the trend of the graph of measured values. However, the interpolated data is volatile. The interpolated values within this line reach a RMS of 7.386 E
The graph is presented with respect to latitude to highlight the area with unfavorable crossover point distribution of figure 3.3 between $[60.75\,^{\circ}, 60.85\,^{\circ}]$. This distribution is most likely the reason for the small amount of sufficient interpolated values. While gradiometric data specifies a sharp rise of vertical gravity gradients within $[60.75\,^{\circ}, 60.85\,^{\circ}]$, the interpolation algorithm is forced to compute contributions of remote points.

Chapter 4

Conclusion

The fact that the European Space Agency grants free access to the satellite data imposes a nearly unrestricted research with this data. The available datasets involve not only altimetric measurements but also comprehensive information about corrections and surface characteristics. Furthermore, ESA provides the user with diverse tools to display or process the information.

The computation method of vertical deflection has been chosen because the orbit of CryoSat provides a rather dense crossover point network. Moreover, the available height data, i.e. the mean sea surface heights, implies a confident handling of the dataset regarding calculating with derivations. However, altimetric crossover point density resolves as insufficient in order to create fine structures of vertical deflections.

The altimetric measurements turned out to be acceptable for interpolation. First, the Matlab-built-in triangulation interpolation method has been tested. This method turned out to yield a rough surface with essentially no outstanding structures within the test region. Furthermore, one must define a grid to use the default interpolation function. Regarding the different densities of both datasets, this condition is greatly restrictive.
In order to fulfill the requirements of interpolating on discrete dataset and creating fine structures the Inverse Distance Weighting Interpolation resolved as a rather reasonable interpolation method. Interpolation onto gradiometric points enables an immediate comparison between measured and calculated vertical gravity gradients.

The outcome provides a rather sparse amount of reasonable interpolated values. One major complication is the distribution of crossover points. The crossover points are aligned in clusters, concentrated to certain regions due to repeat track behaviour. While the distribution is adequate for a low resolution, it is insufficient for creating a set of vertical gravity gradients equivalent to the gradiometric data.

In order to produce low resolution grids of vertical gravity gradients the method of vertical deflection and inverse distance weighting interpolation resolves as acceptable. Utilization of a smart interpolation algorithm enables handling vast amounts of altimetric and gradiometric data.

Outlook

After all, the subject of vertical gravity gradients from satellite altimetry surpasses the extent of one bachelors thesis. The investigated method of vertical deflections resolved as a viable method to produce vertical gravity gradients. However, this method does not utilize the complete along-track data of satellite altimetry but only the intersections of ascending and descending tracks. One interesting aspect is to apply the entire along-track profile data to the large gaps of crossover points within the test region to yield a rather continuous set of vertical gravity gradients. Further, the combination of several altimetric missions might solve the issue of the clustered regions of crossover points. Applying several altimertic datasets will yield a more thorough coverage of ocean surface measurements. This may lead to encouraging results.

Moreover, application of a different method might be a further aspect of investigation. Regarding the behaviour of the frequencies of the derived and measured vertical gravity gradients, a spectral analysis of the altimetric data and the gradiometric data might lead to encouraging aspects.

Bibliography

[CS Mission and Data 2007] European Space Research and Technology Center (ESTEC) **CryoSat: Mission and Data Description** (2007), ESTEC, Noordwijk, Netherlands

[CS Product Handbook 2014] C. Bouzinac **CryoSat Product Handbook** (2014)

[CS Science and Mission 1999] D. Wingham **CryoSat: Science and Mission Requirements** (1999), Department of Space & Climate Physics, University College London, UK

[Footprint 2013] M. Scagliola **CryoSat Footprints** (2013) , ESA Document Reference: XCRY-GSEG-EOPG-TN-13-0013

[Heiskanen/Moritz 1981] W. A. Heiskanen, H. Moritz **Physical Geodesy** (1981), San Francisco, W.H. Freeman and Company

[Heiskanen/Vening-Meinesz 1958] W. A. Heiskanen, F. A. Vening-Meinsez **The Earth and Its Gravity Field** (1958), USA, McGraw-Hill Book Company, Inc.

[Hofmann-Wellenhof/Moritz 2005] B. Hofmann-Wellenhof, H. Moritz **Physical Geodesy** (2005), Wien, Springer

[Roth 2009] M. Roth **Marine Full Tensor Gravity Gradiometry Data Analysis and Euler Deconvolution,** (2009), Bachelor Thesis , University of Stuttgart.

[Sneeuw 2006] N. Sneeuw, **Physical Geodesy,** (2006), Lecture Notes, Institute of Geodesy, University of Stuttgart

[Sandwell 1992] D. T. Sandwell **Antarctic marine gravity fild form high-density satellite altimetry** (1992), Geophsical Journal Int. (1992) 109, p. 437-448

[Torge 1989] W. Torge **Gravimetry** (1989), Berlin, de Gruyter

[Zhao 2012] W. Zhao **Local Gravity Field Modeling by Gradiometry** (2012), Master Thesis, Institute of Geodesy, University of Stuttgart

[CryoSat Mode Mask] Mode Mask for L2 data coverage
Available at: http://cryosat.mssl.ucl.ac.uk/qa/index.html

[Matlab data read] Matlab routines provided by ESA to diget CryoSat data
available on: https://earth.esa.int/web/guest/software-tools/content/-/article/cryosat-matlab-routines

[VisioTerra] http://visioterra.net/VtCryoSat/

Appendix A

Ground Track Velocities

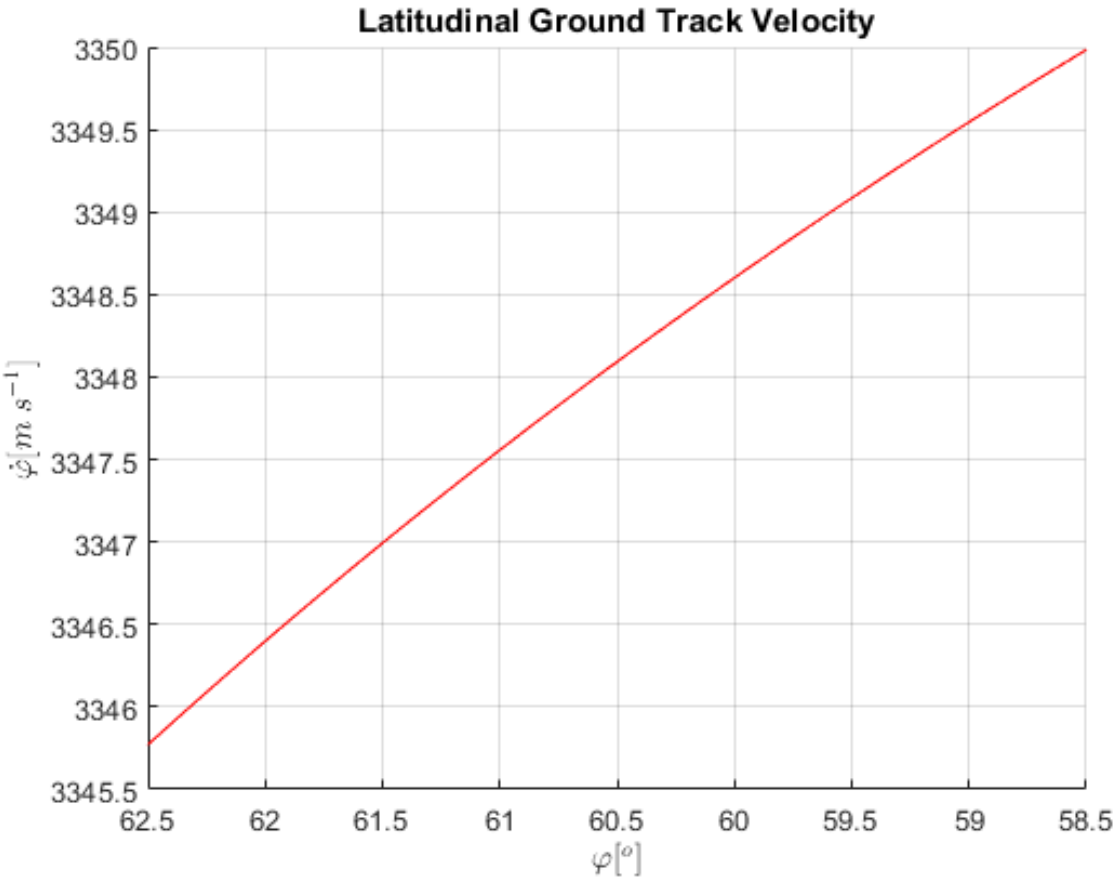

Figure A.1: *Latitudinal ground-track velocities*

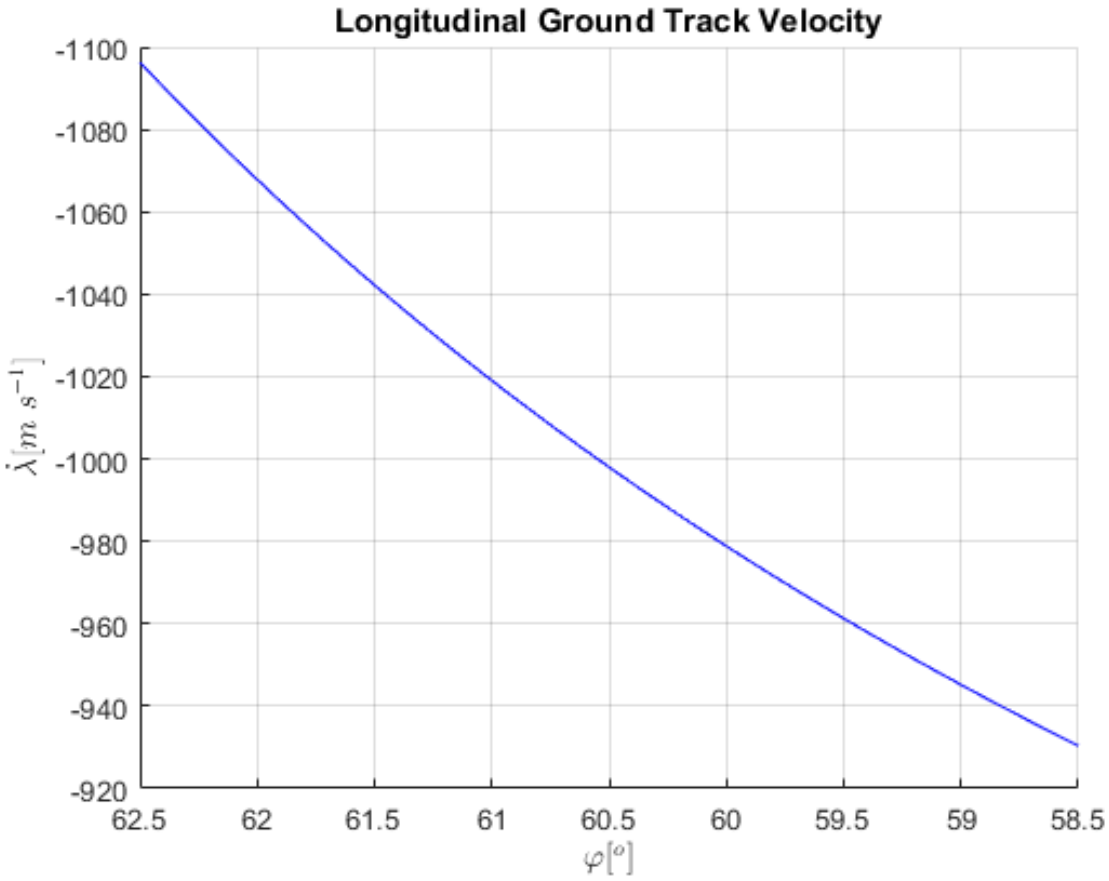

Figure A.2: *Longitudinal ground-track velocities*

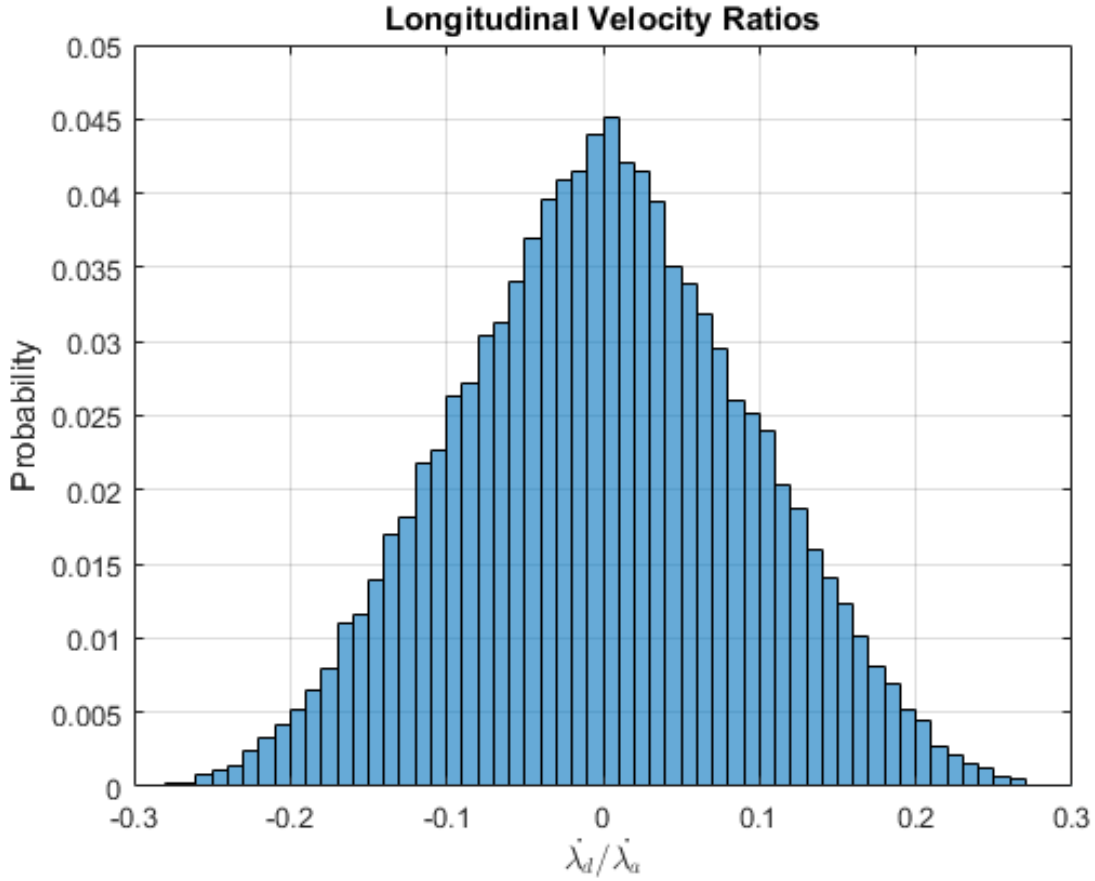

Figure A.3: *Histogram for ratios of ascending and descending longitudinal ground track velocities*

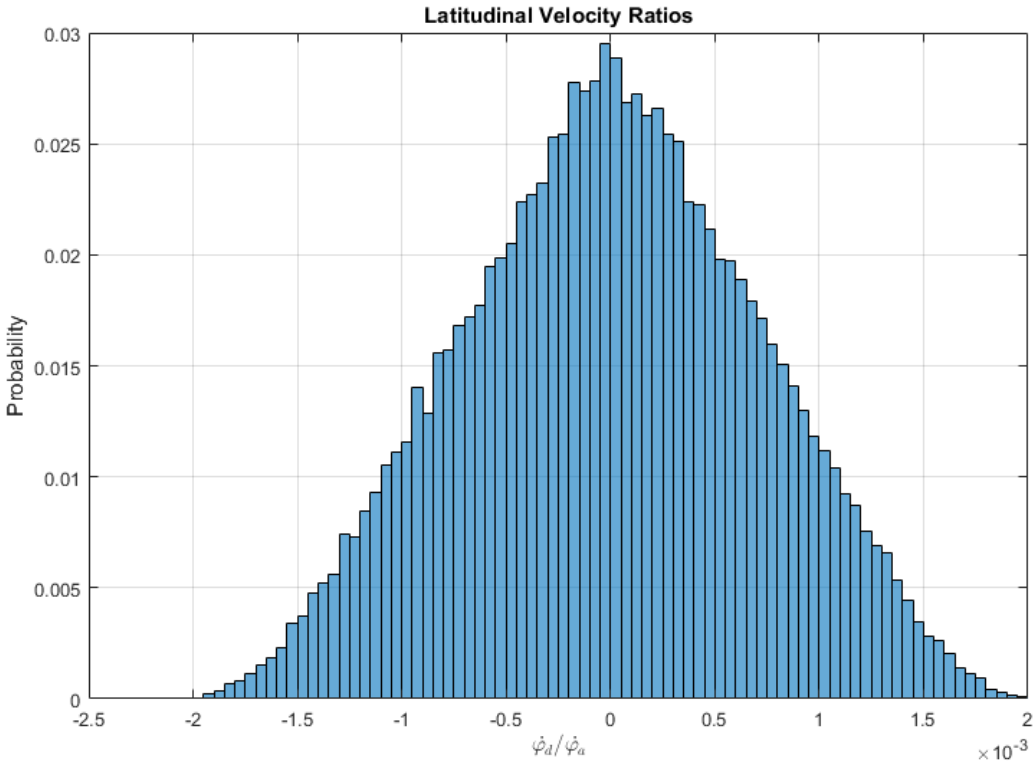

Figure A.4: *Histogram for ratios of ascending and descending latitudinal ground track velocities*

It can be observed, that latitudinal velocities match the condition $\varphi_{\mathrm{a}} = -\varphi_{\mathrm{d}}$ to very accurate degree

$$\mu_{\varphi} = 2.15 \cdot 10^{-6}$$
$$\sigma_{\varphi} = 7.055 \cdot 10^{-4}$$

Although not as accurate as for latitudinal velocities, the relation for longitudinal velocites $\lambda_{\mathrm{a}} = \lambda_{\mathrm{d}}$ still reaches a satisfying degree.

$$\mu_{\lambda} = -3.33 \cdot 10^{-4}$$
$$\sigma_{\lambda} = 0.0929$$